CONF-780941--8

RESONANCE RAMAN SPECTRA OF METAL HALIDE VAPOR COMPLEXES

by

G. N. Paptheodorou

Prepared for

10th Materials Research Symposium on
Characterization of High Temperature Vapors and Gases

National Bureau of Standards
Gaithersburg, Maryland

September 18-22, 1978

UofC-AUA-USDOE

ARGONNE NATIONAL LABORATORY, ARGONNE, ILLINOIS

Operated under Contract W-31-109-Eng-38 for the
U. S. DEPARTMENT OF ENERGY

RESONANCE RAMAN SPECTRA OF METAL HALIDE VAPOR COMPLEXES*

by

G. N. Papatheodorou
Chemical Engineering Division
Argonne National Laboratory
Argonne, Illinois 60439

ABSTRACT

Resonance Raman spectra of complex vapor phase compounds formed by reacting "acidic" gases (A_2X_6 = Al_2Cl_6, Al_2Br_6, In_2Cl_6) with metal halides have been measured. Spectra obtained from equilibrium vapor mixtures of A_2X_6 over solid MX_2 (= $PdCl_2$, $PdBr_2$, $CuCl_2$, $CoBr_2$, $TiCl_2$, $FeCl_2$, $NiCl_2$, $PtCl_2$) were a superposition of the A_2X_6-AX_3 bands and in few cases of new resonance-enhanced polarized bands due to MA_2X_8 and/or MAX_5 complexes. At temperatures above 800 K, characteristic bands due to $MX_2(g)$ (M = Fe, Co, Ni, Cu, Zn) and $M_2X_4(g)$ (M = Cu) were observed. The predominant features of the $PdAl_2Cl_8$, $CuAl_2Cl_8$, and $PdAl_2Br_6$ spectra were three high-intensity, polarized bands which were attributed to the vibrational modes of the complex coupled to the electronic state of the central atom. The spectra of $CuAlCl_5(g)$, $CuInCl_5(g)$ and $Cu_2Cl_4(g)$ species showed resonance enhancement of selective fundamentals which were attributed to vibrational modes of trigonally coordinated Cu(II). Resonance Raman spectra of $U_2Cl_{10}(g)$ and $UCl_5 \cdot AlCl_3(g)$ were characterized by the presence of a strong band attributed to the U-Cl_t stretching frequency. Raman band intensity measurements were carried out for the iron(III) chloride vapors and for the vapor complexes of $CuAl_2Cl_8$, $CuInCl_5$ and $UCl_5 \cdot AlCl_3$ using

*Work performed under the auspices of the Division of Basic Energy Sciences of the U. S. Department of Energy.

different laser powers and frequencies. The measurements suggested increasing spectroscopic temperatures and decomposition of the vapor complexes. The data are discussed in terms of the distribution of vibrational modes and the structure of the vapor species.

I. INTRODUCTION

Reactions of "acidic" halide vapors (*e.g.*, Al_2Cl_6, In_2Cl_6, Fe_2Cl_6) with solid metal halides have been widely investigated by various research groups.[1-6] Spectrophotometric,[2-5] mass spectrometric,[1] and transpiration techniques[1,4,6] have been used to obtain thermodynamic information on these complexes. When the solid is a divalent metal halide, the predominant gaseous complex species is MA_2X_8,[7-12] formed according to the reaction:

$$MX_2(s) + A_2X_6(g) \rightleftarrows MA_2X_8(g) \qquad (1)$$

It has also been found that the acidic gas dimer-monomer equilibrium

$$A_2X_6(g) \rightleftarrows 2AX_3(g) \qquad (2)$$

plays an important role in the stability of these complexes.[5,13,14,15] Thus at high temperatures and/or low pressures, equilibrium (2) shifts to the right and lower molecular weight complexes are formed:

$$MX_2(s) + AX_3(g) \rightleftarrows MAX_5(g) \qquad (3)$$

The absorption spectra of some of these complexes are ligand-field sensitive, and thus yield information about the structure of these types of gaseous molecules. The electronic absorption spectra of $PdAl_2Cl_8$,[7] and $PtAl_2Cl_8$[8] were found to be compatible with square planar coordination of the "central" M(II) ion, whereas for $CoAl_2Cl_8$[3,9] and $CoGa_2Cl_8$,[2] the Co atoms were considered to be octahedrally and/or tetrahedrally coordinated. The electronic absorption spectra of $CrAl_2Cl_8$[11] were interpreted to mean that the transition metal was in distorted octahedral chloride coordination. However, the structural information obtained by absorption

spectroscopy is not conclusive. At elevated temperatures, the bands are broad and their frequencies and/or intensities change drastically with increasing temperature; thus a direct comparison of the spectrum of the gas with known spectra of the solid or solution states is not always possible, and the results are ambiguous.

The present investigation was designed to characterize the structural properties of vapor complexes by means of Raman spectroscopy. Raman spectroscopy has been used successfully in the past to investigate the structures of single-component gases at high temperatures.[16] For the study of complex vapors, however, difficulties arise because, according to Eqs. 1 and 3, the complexes exist only in equilibrium with the monomeric and dimeric acidic vapor. For the equilibrium gas mixture of reactions 1 and 3, $AX_3(g)$ and $A_2X_6(g)$ are the major components and in most cases, the vapor complexes of interest are minor components with partial pressures at least ten times less than those of the carrier gas. Thus, the Raman spectra are expected to be dominated by the bands due to the acidic halide, whereas the bands due to the small amounts of complex will be difficult to recognize. The electronic absorption spectra of most of these M^{+2} ions show bands near the region of the Ar^+ and Kr^+ laser lines; thus it might be possible to enhance the Raman band intensities of the complexes by using resonance Raman techniques.[17]

The results reported in this paper are concerned with the resonance Raman spectra of vapor complexes of aluminum halides (mainly chloride) with transition-metal dihalides. Spectra of vapors in the system M-In-Cl (M = Fe, Co, Ni, Cu, Zn) have been also investigated. At elevated temperatures,

the vapor mixture formed according to reaction 2 and/or 3 also contains vapors of $MX_2(s)$, which in most cases yield resonance Raman and/or strong fluorescence spectra. Thus it was necessary to investigate the spectra of the transition-metal chloride vapors in order to distinguish their vibrational frequencies from those of the vapor complexes.

In addition, the resonance Raman spectra of both uranium pentachloride (U_2Cl_{10}) vapors and of the $UCl_5 \cdot AlCl_3$ vapor complex have been obtained and reported. Finally, the effects of laser power and frequency on the stability of vapor complexes and of iron trichloride vapors have been investigated.

II. EXPERIMENTAL PROCEDURES

High purity "acidic" salts (Al_2Cl_6, Al_2Br_6, In_2Cl_6) were prepared from the corresponding Cerac/Pure Inc. reagent by repeated slow sublimations in fused silica tubes under vacuum. The palladium(II) halides were purchased from Mathey Bishop Inc. Other anhydrous transition-metal chlorides were prepared by dehydrating $MX_2 \cdot XH_2O$ (Baker A.R) in vacuum and/or in gaseous HCl atmosphere at elevated temperatures. A final purification of the metal halide salts was made by vapor-transporting them according to reactions 1 and 3 with the use of the corresponding "acidic" vapor halide. The UCl_5 was synthesized from UO_2, aluminum chloride and Cl_2 at 300°C according to the reaction:

$$6UO_2(s) + 4Al_2Cl_6\left(\begin{matrix} g \\ \ell \end{matrix}\right) + 3Cl_2(g) \longrightarrow 4Al_2O_3(s) + 6UCl_5(s) \qquad (4)$$

The $UCl_5(s)$ was further purified by vapor complex transport across a temperature gradient[18] in the presence of excess Al_2Cl_6.

Raman spectra were excited using either a Coherent Radiation argon or Krypton ion laser, or a Coherent Radiation dye laser pumped by a 15 watt Control Laser Corporation argon laser. The scattered light was analyzed at 90° with a Spex 1400 or a Jobin-Yvon HG-2S double monochromator, Channeltron phototube, and PAR(SSR) photon counting electronics or PAR chopper lock-in amplifier electronics. Figure 1 shows the optics of the laser Raman system designed for use at high temperatures. To obtain the high-temperature gaseous spectra, a nichrome-wire dual-winding water-cooled optical furnace was constructed. The furnace was equipped with a chromel alumel thermocouple for monitoring the temperature and had an effective collection aperture of f 1.0. The furnace temperature gradients could be adjusted so that the window openings were always 5 to 10°C hotter than the remaining part of the furnace. These temperature gradients permitted studies of vapors in equilibrium with a solid and kept the solid away from the optical paths. A schematic of the furnace is shown in Fig. 2.

The optical cells containing salt vapors with pressures less than 5 atm were made of fused silica tubing (20 mm OD, 18 mm ID and 2.5 to 5 cm long). For vapors having pressures above 5 atm, tubing of 3-mm wall thickness was used. Preweighed amounts of the chemicals were transferred into a dry and degassed cell of known volume V. The cell was sealed under vacuum and attached to a fused silica manipulation rod. The "ideal gas" pressure P_o of undissociated A_2X_6 at temperature T was calculated from the equation $P_o = nRT/V$, where n is the number of moles of A_2X_6 added to the Raman cell and R is the gas constant.

To prepare samples with no excess of $MX_2(s)$, a modified cell having a side tube was used. A chunk of $MX_2(s)$ was placed into the side tube and equilibrated with the A_2X_6 at a temperature ~50° above the sublimation point of the acidic halide. The cell was then quickly cooled to solidify the gases present away from the solid. Finally, the remaining excess $MX_2(s)$ was removed from the cell by sealing off the side tube. For each system studied several (3-8) different cells were made.

Two polarization configurations were used to record the Raman spectra; one was designated as $\perp$, $\perp$, the other as $\parallel$, $\perp$. Thus, $I_{\perp,\perp}$ is the Raman intensity measured with both the incident radiation and scattered radiation polarized perpendicularly to the scattering plane, whereas $I_{\parallel,\perp}$ is the Raman intensity measured with the incident radiation analyzed perpendicular to the scattering plane.

The optical cells were placed inside the mechanically stable metal core of the furnace and were always in a fixed position relative to the collecting lens and/or entrance slit. A cell was first introduced in the optical furnace and the intensity of the scattered light was "maximized" by positioning the focusing and collecting lenses with two x, y, z micropositioners. After obtaining the spectra, the cell could be removed and cooled to room temperature and then reintroduced into the optical furnace, yielding always, with no further microspositioner adjustments, the same Raman intensity. Thus, by using the same laser power, the Raman intensities were reproduced to within less than 5% and

the relative Raman intensities of gases at different temperatures and pressures could be obtained within the same error.[19]

III. COMPLEXES OF ALUMINUM-TRANSITION METAL HALIDES

Table I shows the various aluminum halide-MX_2 systems investigated by Raman spectroscopy. Only three out of nine systems gave bands attributable to the vapor complexes. The spectra of all other systems were dominated by the Raman bands of the "acidic" gas present in the cell.

The electronic absorption spectra of these vapor complexes showed ligand field bands which in most cases overlapped with the frequency region of the lasers used. Examples of such spectra are shown in Fig. 3 for the nd^8 transition-metal complexes. The frequency region of the laser lines used is indicated by the vertical lines. In the presence of a high concentration of complex, the laser beam(s) was strongly absorbed giving very weak signals. Therefore, it was necessary to adjust the temperature and the "acidic" gas pressure by trial and error to find the optimum partial pressure of the complex which would allow the beam to go through the vapors and at the same time give rise to Raman signals. Cells with and without an excess of $MX_2(s)$ were examined at pressures of A_2X_6 from ~0.1 to 28 atm. It was found that best cells for achieving a high signal-to-noise ratio and a high ratio of vapor complex-to-"acidic" gas signals were those with no excess $MX_2(s)$, having low partial pressures (less than 0.1 atm) of complex.

Palladium Complexes: $PdAl_2Cl_8$; $PdAl_2Br_8$. Figures 4 and 5 show representative Raman spectra of $PdAl_2Cl_8$-Al_2Cl_6-$AlCl_3$ and of the $PdAl_2Br_6$-Al_2Br_6-$AlBr_3$ gas mixtures excited with the 647.1 and 488.0 nm laser lines from a cell with

$P_{complex}$ ~0.3 and ~0.10 atm, respectively. Comparison with the spectra of pure aluminum halide vapors[15] reveals that some new bands are superimposed on the Al_2X_6-AlX_3 modes. These new bands are attributed to $PdAl_2X_8$ and are listed in Table II. The three strong polarized bands I, II, III, marked as a, c, and d on Figs. 4 and 5, were present in all spectra taken with different excitation lines at different temperatures and pressures. The intensities of bands a, c and d measured from spectra exited with the "red" laser lines are similar in magnitude to those of $Al_2X_6(g)$ polarized fundamentals. The pressure ratio of Al_2X_6 to $PdAl_2X_8$, however, is ~10/1; thus it seems that the bands due to the complex exhibit preresonance enhancement.

At constant values of T and $P_{Al_2X_6}$, the intensities of bands a, c and d, relative to the intensities of the Al_2X_6 bands were found to vary with the frequency of the excitation line. This is shown quantitatively in Fig. 1, for the $PdAl_2Cl_8(g)$ species where the relative intensities of band d to the 218 cm^{-1} band of Al_2Cl_6, are plotted *vs* the laser excitation frequencies. Excitation profiles calculated for bands a and c were similar to the excitation profile of band d, but had larger experimental uncertainty.

This phenomenon is analogous to that observed for the $\nu_1(A_{1g})$ mode of square planar MX_4^{-2} and octahedral MX_6^{-4} complexes.[25-27] Stein *et al.*[26] have shown how de-enhancement of the symmetric stretch intensity arises in these complexes from interference between weak scattering from Laporte-forbidden electronic states and strong preresonance scattering from higher energy allowed charge-transfer states. A theoretical description of the same effect has been also given by Zgierski.[28]

Assuming that two electronic states $|s\rangle$ and $|e\rangle$ are well separated, then the transition moments from the ground state $|g\rangle$ to these states are

$$\langle g|\vec{M}|s\rangle = \vec{M}_{gs} \tag{5}$$

$$\langle g|\vec{M}|e\rangle = \vec{M}_{ge} \tag{6}$$

For an electronically allowed transition, both transition moments are different from zero, and the preresonance Raman intensity of a fundamental with Raman shift ν_f is proportional to the A and/or B terms of Albrecht's theory.[17]

$$I_s(\nu_f) \sim A_s \sim (\nu_o - \nu_f)^4 \left[\frac{(\nu_s^2 - \nu_o^2)}{(\nu_s^2 - \nu_o^2)^2}\right]^2 \tag{7}$$

$$I_{se}(\nu_f) \sim B_{es} \sim (\nu_o - \nu_f)^4 \left[\frac{(\nu_s\nu_e + \nu^2)}{(\nu_s^2 - \nu_o^2)(\nu_e^2 - \nu_o^2)}\right]^2 \tag{8}$$

Apart from the frequency-dependent part, the A terms involve vibrational interaction with the $|s\rangle$ (or $|e\rangle$) state by way of Franck-Gordon overlap integrals, and only totally symmetric vibrations are resonance enhanced. The B terms, on the other hand, involve Herzberg-Teller vibronic mixing of the two exited electronic states $|s\rangle$ and $|e\rangle$, and all vibrational modes having any symmetry, which is contained in the direct product of the representations of the two electronic states, are resonance-enhanced.

If states $|g\rangle$ and $|s\rangle$ are of different parity, then the transition moment $\vec{M}_{gs} = 0$ (Laporte forbidden) and the Raman intensities of totally symmetric modes do not show resonance enhancement, using the A_s term. It has been shown,[14-20] however, that the Raman intensity of totally symmetric modes can be derived from preresonance enhancement using both the B_{es} term

and the A_e term of the electronically allowed higher energy state $|e\rangle$. The Raman excitation profile is then proportional to

$$I(\nu_f) \sim \frac{1}{(\nu_e - \nu_o - i\Gamma_e)^2} + R^\circ \frac{1}{(\nu_e - \nu_o - i\Gamma_e)(\nu_s - \nu_o - i\Gamma_e)} \qquad (9)$$

where R° is the ratio of the I_{es} to I_e Raman intensities. As the laser frequency, ν_o, is swept through the frequency of the forbidden state, ν_s, the second term of the above equation changes sign and the Raman intensity of a totally symmetric fundamental is de-enhanced.

Presumably the three polarized modes of $PdAl_2X_8$ are coupled to the ligand field and charge-transfer electronic states of Pd(II) exhibiting the de-enhancement of the resonance Raman intensity described by eq. 9.

The frequency of band d is far below a Pd-X_t (terminal) frequency and lies below the ν_2 fundamental of $Al_2X_6(g)$ which describes a bridged $\nu_{Al\text{-}X_b}$ mode. Thus, it is reasonable to assume that the Pd atom in the $PdAl_2X_8$ is attached only to X-bridged halide atoms. Figure 6 shows three different molecular structures with the central ion bound to four or six X atoms. The number of polarized Raman bands, A_1, expected from these molecules are: Molecule a, 4; Molecule b, 5; Molecule c, 5.

The electronic states of Pd(II) in these molecules are affected both by the geometric arrangement of the X atoms and, to some extent, by the neighboring Al(III) atoms.[29] Thus, the three A_1 (resonance Raman) modes of $PdAl_2X_8$ probably arise from the structural geometry of Pd(II) that includes the Al(III) atoms. There are three A_1 species arising from these central atom geometries. These species are likely to show resonance

enhancement due to coupling with the electronic states of the central atom. Thus the polarized modes can be specified as follows:

$$\Gamma_{mol.\underline{a}} = A_{1g}(R) + 3\,A_{1g}(R,rR)$$

$$\Gamma_{mol.\underline{b}} = 2\,A_{1g}(R) + 3\,A_{1}(R,rR) \qquad (10)$$

$$\Gamma_{mol.\underline{c}} = 2\,A_{1g}(R) + 3\,A_{1g}(R,rR)$$

where rR and R indicate resonance Raman and Raman activity, respectively. Evidently, no distinction between molecules a, b, and c can be made, on the basis of these $A_1(R,rR)$ modes alone. However, from previous studies,[25,26,17] it appears that the de-enhancement of the symmetric fundamentals in the region of the d→d electronic bands is a characteristic of "centrosymmetric complexes." Excitation of non-centrosymmetric tetrahedral $CoCl_4^{-2}$ and $CoBr_4^{-2}$ complexes within the $^4A_2 \rightarrow {}^4T(P)$ absorption band gives rise to resonance enhancement of the Co-X stretching fundamental.[30] This is probably due to the fact that, in centrosymmetric complexes, the d→d transitions are strictly Laporte-forbidden, whereas for non-centrosymmetric complexes the ligand field transitions are partially allowed by d-p mixing and thus the $\vec{M}_{gs}$ in Eq. 5 does not vanish. These considerations and the observed minimum in the excitation profile of $PdAl_2X_8$ suggest that the central Pd(II) atom possesses a center of symmetry in this molecule. Thus, structure c and/or strongly distorted structures a or b are excluded.

A distinction between the two structures, a and b can be made from the proximity of the d band of $PdAl_2X_8(g)$ to the ν_1 (A_{1g}) mode of square planar

PdX_4^{-2} in K_2PdX_4.[31] Thus structure b, having the Pd(II) in a square planar arrangement is the most probable one. The assignment of the three strong polarized modes observed in the spectra is given in the last column of Table II.

The intensities of bands a, c and d, relative to the aluminum halide bands, were found to change with the power of the excitation line. Doubling the 488.0 nm line power from 450 to 900 mW increased the ν_1 intensity of the AlX_3 monomer. It is thus possible that the absorption of the laser line by the d→d band gives rise to an increasing spectroscopic temperature and/or to a partial photodissociation of the complex:

$$PdAl_2X_8(g) \xrightarrow{h\nu} PdX_2 \cdot kAlX_3(g) + (2 - k)\ AlX_3(g)$$

Such a scheme alters the measurements of the relative intensities of the complex, and corrections should be made for the calculation of the excitation profile. However, due to the large intensity changes of the $PdAl_2X_8$ bands observed as the excitation line is changed from 647.1 to 488.0 to 457.9 nm, these corrections are not large enough to alter the minimum in the excitation profile (Fig. 3).

Copper Complexes: $CuAl_2Cl_8$, $CuAlCl_5$. The temperature dependence of the electronic absorption spectra of the Cu-Al-Cl system has been measured.[23] At lower temperatures, the spectra of the "yellow" gaseous complex(es) are characterized by a d→d band of low molar absorptivity (∿80 liter/mol·cm) at 11.7 kK and three charge-transfer bands at 30.5, 38 (shoulder band), and 47.5 kK. In the temperature range from 445 to ∿575 K the molar absorptivity of the d→d band is independent of temperature. At temperatures above 575 K,

the molar absorptivity at 11.7 kK decreases with increasing temperature, a new band arises at 20 kK, and the color of the gaseous complex(es) changes from "yellow" to "red". All laser lines used to obtain the Raman spectra lie between the Cu(II) d→d band and the Cu→Cl change transfer band. At high temperatures the Ar^+ laser lines were superimposed on the ∿20 kK "red" species band.

Figure 7 shows the Raman spectra obtained at 575 K, with different excitation lines, from a cell containing ∿0.3 atm of aluminum chloride and ∿0.05 atm of copper gaseous complex. The predominant features of the spectra obtained with the red 647.1 nm line are the Al_2Cl_6 bands and four weak bands, namely, a (84.5 cm^{-1}), c (175 cm^{-1}), d (281 cm^{-1}) and f (448 cm^{-1}), whose intensities were found to increase with increasing temperature and frequency of the excitation line.

As the laser lines change from red to blue, the intensities of the a, c, and d bands increase relative to the intensities of the Al_2Cl_6 bands but not as fast as the intensity of band f. A new strong band (e) appears at 291 cm^{-1}, and its intensity increases proportionately to the intensity of band f. Furthermore, a series of combination and overtone bands appears in the spectra excited with the Ar^+ laser lines. Most of these bands can be accounted for in terms of overtones and combinations of the e and f bands. No combinations or overtones including a, c, and d bands are present in the spectra.

Further variations of the intensities of the Raman spectra result from changing either the power (intensity) of the excitation line at constant

temperature or the furnace temperature at constant excitation line. Experiments designed to measure the effect of aluminum chloride pressure show that the intensities of band e and f decrease markedly with decreasing aluminum chloride pressure. These changes for the f band are shown in Fig. 8. The intensity of band e was also diminished in the high pressure cell with band d having the predominant intensity in the 270 to 300 cm^{-1} region. Bands a and c could be also recognized in the high pressure cell and their intensities slightly increased with increasing aluminum chloride pressure.

All observations are best interpreted to indicate that that the Raman spectra can be accounted for in terms of two gaseous copper species. The bands a, c, and d, exhibiting preresonance Raman enhancement of their intensities, are attributed to the $CuAl_2Cl_8$ gaseous molecule, which presumably has a structure similar to a, b, or c as presented in Fig. 6. The high intensity bands, e and f, and their combinations and overtones are attributed to the resonance-enhanced Raman bands of a "new" species.

At this point, it should be noted that the temperature dependence of the absorption spectra (Ref. 23) is indicative of a two-species equilibrium, in which the band at 11.7 kK is mainly associated with the "yellow" species and the band at 20 kK is associated with the high-temperature "red" species. It thus appears that the increasing intensity of the e and f Raman bands is related to the presence and increasing intensity of the 20 kK electronic transition and that the "new" species arises from a decomposition of the $CuAl_2Cl_8$ molecule. A possible decomposition scheme, analogous to that found[14] for the $CoIn_2Cl_8$ and $PdIn_2Cl_8$ complexes, is as follows:

$$CuAl_2Cl_8(g) \rightleftarrows CuAlCl_5(g) + AlCl_3(g)$$

Choosing a possible structure (Fig. 6) for the $CuAl_2Cl_8$ molecule is difficult. Similarities between the $Cu\text{-}Cl_b$ frequency and frequencies of other copper chlorides of known structure cannot be used in the selection since the Cu(II) exhibits strong Jahn-Teller distortions and all its halide compounds have strongly distorted octahedral or tetrahedral coordinations.

Based on the electronic absorption spectra, Sutakshuto[22] proposed a distorted octahedral coordination for the Cu(II) in $CuAl_2Cl_8$ and a structure similar to a in Fig. 6. The observed $\nu_{Cu\text{-}Cl_b}$ frequency (281 cm^{-1}) for the gaseous complex lies below the 297 cm^{-1} value for $CuCl_4^{-2}$ in distorted tetrahedral coordination[32] and is in support of a distorted structure a. On the other hand, the ring deformation ($\sim$84 cm^{-1}) and angle bending ($\sim$175 cm^{-1}) modes are the same for both the $PdAl_2Cl_8$ and $CuAl_2Cl_8$ complexes (Table II) and thus a square planar structure (structure b) is also acceptable.

The structure of the $CuAlCl_5$ species is shown in Fig. 9. It is noteworthy that the 448 and 291 cm^{-1} bands are, respectively, very close to the Cu-Cl and Cu-Cl frequencies of trigonally coordinated copper. (Table III and section IV).

Cobalt Complexes: $CoAl_2Cl_8$, $CoAl_2Br_8$. Cells having a variety of concentrations of the vapor complexes and with pressures of $Al_2X_6(g)$ up to 28 atm have been investigated. Both right angle and backscattering techniques have been used with all available laser lines. The scattered light, however, shows

only the presence of the Al_2X_6-AlX_3 bands and no bands due to the complexes. The relative concentrations of $CoAl_2X_6(g)$ and $Al_2X_6(g)$ were similar to those in the Cu-Al-Cl and Pd-Al-X systems, but no resonance enchancement of the cobalt complex fundamentals was observed.

The change transfer bands of the $CoAl_2X_6$ complexes are at higher energies[5,9] than those of the Cu or Pd complexes and do not overlap with the d→d bands. The laser lines used to excite the spectra cover part of the d→d bands but are far away from the CT band. Presumably, neither preresonance enhancement (eq. 7) nor destructive interference effects (eq. 9) can occur for these vapors.

As noted above, however, non-centrosymmetric CoX_4^{-2} shows resonance enhancement of its Raman fundamentals by involving the d-p mixing of the ligand field transitions.[30] It is thus possible that the absence of vapor complex bands from the Co-Al-X spectra arises from a near centrosymmetric coordination of Co in the $CoAl_2X_8$ complex. This conclusion is tentative and questionable since other factors (*e.g.*, laser decomposition of complex; see section VI) might also prevent detection of vapor complex bands.

Complexes with Ti, Fe, Ni and Pt. As in the case of the $CoAl_2X_8(g)$, no Raman signals were obtained for the MAl_2Cl_8(M = Ti, Fe, Ni, Pt) complexes, although many cells have been thoroughly investigated at different temperatures, pressures and laser excitation lines. It has been demonstrated by spectrophotometric[8,20] and transpiration[6] techniques that these complexes have lower partial pressures than those for the Pd, Cu, and Co complexes. Thus it

is possible that the very small amounts of complexes present in the cells and/or their high energy CT bands (*e.g.*, the ~48 kK band for $NiAl_2Cl_8$; Fig. 3) may account for very weak Raman signals which are completely obscured by the Al_2Cl_8 bands.

IV. COMPLEXES OF INDIUM-TRANSITION METAL CHLORIDES

Recent spectrophotometric[13,14] and mass spectrometric[33] studies have shown that the predominant vapor species of the indium complexes are formed according to reaction 3. In the present section our attempts to obtain the Raman spectra of M-In-Cl (M = Fe, Co, Ni, Cu, Zn) vapor complexes are reported. For these studies, temperatures near or above the sublimation point of indium chloride are required; at these temperatures, the vapors from the MCl_2 solids interfere with the spectra of the other vapor components. Thus, in order to distinguish the complex Raman active bands from those of the other gases, a detailed knowledge of both the In_2Cl_6-$InCl_3$ and the MCl_2 vapor spectra are required. The temperature and pressure dependence of the indium chloride vapor spectra have been obtained and part of the results have been reported elsewhere.[21] The spectra obtained for the MCl_2(M = Fe, Co, Ni, Cu, Zn) vapors are outlined briefly here.

$ZnCl_2$, $FeCl_2$. Raman spectra of these vapors were obtained in the temperature range from 900 to 1150 K. Each spectrum was characterized by a single, strong polarized band. Figure 10 shows characteristic spectra for the zinc chloride vapors. The spectra for iron(II) chloride were similar but were superimposed on a broad fluorescence background. The frequencies measured from the spectra are listed in Table IV and are assigned to stretching modes of linear triatomic molecules.

$CuCl_2$. The temperature dependence of copper(II) chloride vapor spectra, obtained from a cell containing no excess of $CuCl_2(s)$, is shown in Fig. 11. Spectra were also measured using different excitation lines and different laser intensities. The resonance Raman character of the spectra are evident from the strong scattering signals observed, the variation of the relative Raman intensities with excitation frequency, and the progression of combination-overtones. Three bands (Table IV) and their combinations and overtones were found to increase in intensity with increasing temperature. Three other bands, at 314, 442 and 545 cm^{-1}, decrease in intensity with increasing temperature.

The observed changes are best interpreted in terms of a dimer-monomer equilibrium:

$$Cu_2Cl_4(g) \rightleftarrows 2\ CuCl_2(g) \qquad (11)$$

The three bands listed in Table IV were assigned to the $\nu_1(A_1)$, $\nu_2(A_1)$ and $\nu_3(B_1)$ fundamentals of a bent C_{2v} triatomic molecule. A strong band at 250 cm^{-1} is assigned to a difference band $\nu_1 - \nu_2$. Bands with frequencies above 600 cm^{-1} were combinations of overtones of the three $CuCl_2(g)$ fundamentals.

As indicated in Table III, the fundamentals observed for the $Cu_2Cl_4(g)$ are assigned to the $Cu\text{-}Cl_t$ and $Cu\text{-}Cl_b$ modes of the copper in a trigonal configuration having one terminal chloride and two bridged ones (Fig. 9).

$NiCl_2$, $CoCl_2$. High temperature (resonance) fluorescence spectra were observed from these vapors. Figure 12 illustrates the $NiCl_2(g)$ spectrum from cells containing no excess of solid at 900 K. Increasing the temperature did not alter the relative intensities of the bands. The complicated nature of the spectrum, showing many overlapping bands, will not be discussed in detail. However, it should be noted that the intense bands observed for $NiCl_2$ at wave numbers below 19,500 cm^{-1} were multiplets and/or combinations of two basic frequencies at 362 and 170 cm^{-1}. The $CoCl_2$ spectra were also characterized by two basic frequencies, of 359 and 177 cm^{-1}.

A possible assignment of the 362 cm^{-1} ($NiCl_2$) and 359 cm^{-1} ($CoCl_2$) frequencies is the ν_1 symmetric stretch for the triatomic molecules. The proximity of these values to the ν_1 value of $ZnCl_2(g)$, $FeCl_2(g)$ and $CuCl_2(g)$ (Table IV), and the previously measured ν_1 value for $NiCl_2$ (340-370 cm^{-1})[34,35] are in support of such assignment. The 170 cm^{-1}($NiCl_2$) and 177 cm^{-1}($CoCl_2$) frequencies may arise from the ν_2 mode, but the values are much higher than the frequencies observed by low temperature IR matrix isolation techniques[36] (85 and 95 cm^{-1} respectively). The differences are probably due to changes in structure between the high and low temperature molecules. Thus the assignments given in Table IV for $NiCl_2$ and $CoCl_2$ should be considered tentative.

For the investigation of the M-In-Cl complexes, a series of Raman cells having various partial pressures of the complex and various In_2Cl_6-$InCl_3$ pressures have been made. From all the systems studied (M = Fe, Co, Ni, Cu, Zn), only the Cu-In-Cl vapors gave rise to resonance Raman signals which could be attributed to vapor complexes. Spectra obtained from Zn-In-Cl and Fe-In-Cl consisted of a superposition of the indium chloride fundamentals and the symmetric stretch of the MCl_2 triatomic molecule. At temperatures above 1000 K,

the Co-In-Cl and Ni-In-Cl spectra were obscured by the fluorescence spectra of $NiCl_2(g)$ and $CoCl_2(g)$, respectively. At lower temperatures, where the MCl_2 pressures were very low, only the characteristic indium chloride frequencies were observed. Measurements of the relative Raman intensities have shown that more $InCl_3(g)$ monomer was present in the cells containing the complex than in the cells having only indium chloride. The amounts of indium chloride added in both types of cells were calculated to create equal indium chloride pressures. Furthermore, it was found that the amount of $InCl_3(g)$ in the cells containing the complex increased with increasing laser power and laser frequency. These observations may imply that the laser beam either increased the spectroscopic temperature in the M-In-Cl cells and shifted the monomer-dimer equilibrium or resulted to a photodissociation of the $MInCl_5$ complex:

$$MInCl_5(g) \rightarrow MCl_2(g) + InCl_3(g) \qquad (12)$$

Both schemes increase the amounts of $InCl_3(g)$ and are similar to the dissociation schemes discussed in the last section of this paper. It appears that the lack of obtaining spectra from the M-In-Cl complexes ($M \neq Cu$) is mainly due to their low stability and to complications arising from the presence of strong $MCl_2(g)$ and indium chloride bands in the spectra which obscure the vapor complex bands.

$CuInCl_5$. Figure 13 shows the Raman spectra obtained from a Cu-In-Cl cell containing no $CuCl_2(s)$ excess. The spectra are characterized by bands due to the $InCl_3$-In_2Cl_6 modes and by two strong bands at 442 and 300 cm^{-1} and their overtones and combinations which are attributed to the vapor complex modes. In Table III the frequencies of the observed fundamentals are compared to those of $CuInCl_5$,

and an assignment based on a trigonally coordinated copper is given. Thermodynamic considerations[37] have suggested a $CuInCl_5$ stoichiometry for the vapor complex and the data in Table III can be best interpreted to support a structure similar to that proposed in Fig. 9. Measurements of spectra obtained from the same cell have shown that the intensities of the copper complex, relative to those of indium chloride, increase with increasing frequency of laser excitation. These changes and the appearance of strong combinations and overtones are characteristics of the resonance Raman nature of the spectra. The other distinct bands seen in the spectra were attributed to the In_2Cl_6-$InCl_3$ gas fundamentals. It is noteworthy however that the $InCl_3(g)$ bands ν_1 ($InCl_3$) = 350 cm^{-1} and $\nu_4(InCl_3)$ = 95 cm^{-1} are the dominant bands indicating that the monomer is the major component. Spectra of pure indium chloride vapors obtained at similar pressures and temperature show intense $In_2Cl_6(g)$ dimer bands.

The temperature dependence of the Cu-In-Cl spectra (no $CuCl_2$ excess) is shown in Fig. 14. The spectra are dominated by the $InCl_3(g)$ fundamentals and by the $CuInCl_5$ bands. The relative intensities of the $\nu_1(InCl_3)$ and $\nu_{Cu\text{-}Cl_t}$ ($CuInCl_5$) change dramatically with increasing temperature and new bands arise at higher temperatures. The changes can be easily recognized by comparison with the $CuCl_2(g)$ spectra (Fig. 11). It appears that the 970 K spectrum is mainly a superposition of the $InCl_3(g)$ and $CuCl_2(g)$ spectra and that the dissociation reaction 12 can account for the large temperature-dependent features observed in Fig. 14. It must be emphasized, however, that the decomposition may be induced by the laser beam and/or by the increasing furnace temperature.

V. URANIUM(V)-ALUMINUM CHLORIDE VAPORS

Spectrophotometric[38] and mass spectrometric[39] studies have shown that UCl_4 reacts in the presence of chlorine with aluminum chloride to form a volatile vapor complex:

$$2UCl_4(s) + Cl_2(g) + Al_2Cl_6(g) \rightarrow 2UCl_5 \cdot AlCl_3(g) \qquad (13)$$

In the absence of aluminum chloride, the chlorination of UCl_4 yields a rather volatile UCl_5 dimer:

$$2UCl_4(s) + Cl_2(g) \rightarrow U_2Cl_{10}(g) \qquad (14)$$

whose stability decreases with increasing temperature.[38,39] The present section is concerned with the Raman spectra of vapors formed according to reactions 13 and 14. Raman cells were made using either $UCl_4(g)$ and $Cl_2(g)$ or $U_2Cl_{10}(s)$. In early experiments, it was found that the laser lines from ∿640.0 to 457.9 nm were strongly absorbed by both the $U_2Cl_{10}(g)$ and $UCl_5 \cdot AlCl_3(g)$ vapors, which in this energy region possess strong CT bands.[38] It was also found that the use of high-power laser lines at temperature above ∿520 K reversed reactions 13 and 14 yielding solid UCl_4, which was deposited on the cell wall and consequently blocked the passage of the beam. It was possible however to obtain Raman spectra of both uranium gases from cells having low partial pressures and no solid present.

For investigating $U_2Cl_{10}(g)$, it was necessary to introduce ∿2 atm of Cl_2 into a cell containing small amounts of UCl_4 or U_2Cl_{10} solids and to use furnace temperatures less than 500 K. The cells for the $UCl_5 \cdot AlCl_3$ studies were made from U_2Cl_{10} and Al_2Cl_6, without or with Cl_2 present; measurements could be made up to 720 K. It appeared that the formation of $UCl_5 \cdot AlCl_3$ not only enhanced the $U_2Cl_{10}(s)$ volatility but also raised the stability of the pentavalent state in the complex relative to that in pure $U_2Cl_{10}(g)$.

The Raman spectra of the U_2Cl_{10}-Cl_2 vapors are presented in Fig. 15. Superimposed on the pure rotational and vibrational-rotational contours of Cl_2 is a strong polarized band at 354.5 cm^{-1} and its overtone, both of which are attributed to $U_2Cl_{10}(g)$. No other bands were observed, although recently reported spectra of U_2Cl_{10} in dichloromethane show, apart from an A_g mode at 367 cm^{-1}, two other polarized bands at 324 and 130 cm^{-1}. The structure of U_2Cl_{10} (Fig. 16) is presumed to be two octahedra sharing an edge. The point group of the molecule is D_{2h} and six polarized, A_g, Raman active modes are expected. From the thermodynamics of reaction 14, the partial pressure of U_2Cl_{10} in the Raman cell is estimated to ∿0.001 atm. This low partial pressure may explain the absence of other (weaker) Raman bands from the spectra and suggests that the intensities of the observed mode and overtone are enhanced by resonance conditions. The 354.5 cm^{-1} frequency is close to the stretching frequency observed in the solid (365 cm^{-1}) and lies between the A_{1g} modes of UCl_6 (∿370 cm^{-1}) and UCl_6 (∿340 cm^{-1}). The observed band is thus assigned to the U-Cl_t stretching of the U_2Cl_{10} molecule.

The upper part of Fig. 15 presents the spectra obtained from a U(V)-Al-Cl cell in which the partial pressure of the vapor complex was ∿0.003 atm (at 500 K). At temperatures above 480 K no solid phases could be visually detected in the cell. Superimposed on the aluminum chloride bands is one sharp band at 362 cm^{-1} which is presumably due to $UCl_5 \cdot AlCl_3(g)$. A weak peak at ∿560 cm^{-1} is due to small amounts of Cl_2 which probably resulted from partial decomposition of U_2Cl_{10} during the cell preparation.

Repeated measurements of $UCl_5 \cdot AlCl_3$ have established a band frequency of 362 ±1 cm^{-1}, a value that is ∿7 cm^{-1} higher than the 354.5 cm^{-1} band observed for

$U_2Cl_{10}(g)$. Adapting the molecular structure shown in Fig. 16 the new band is assigned to the U-Cl_t stretching frequency. The 7 cm^{-1} difference between the $UCl_5 \cdot AlCl_3$ and U_2Cl_{10} bands is probably due to the higher polarizing power of the aluminum as counter cation in the complex, relative to that of uranium as counter cation in the dimer. There are 24 vibrational modes for the $UCl_5 \cdot AlCl_3$ molecule and their distribution for a C_{2v} point symmetry is

$$\Gamma = 9A_1 + 3A_2 + 6B_1 + 6B_2$$

All modes are Raman active but, as in the case of $U_2Cl_{10}(g)$, only one strong resonance Raman band is observed in the spectrum.

Changes in frequency of the excitation line produced changes in intensity of the 362 cm^{-1} band relative to the aluminum chloride bands. On changing the excitation frequency from 457.9 to 501.7 nm, the $UCl_5 \cdot AlCl_3$ intensity increased relative to that of Al_2Cl_6 (see Fig. 17). However, further changes toward the blue lines resulted in decreasing intensities. This behavior suggests an excitation profile for the 362 cm^{-1} band with a maximum near 500 nm. The absorption spectra of the complex[38] show that a strong CT band starts at ~700 nm but, due to the high molar absorptivity, the maximum of the band(s) has not been seen. Without taking into account any resonance Raman interference phenomena,[28] the maximum of an electronically allowed transition is expected to coincide approximately with that of the excitation profile. Thus it is possible that the maximum of the vapor complex CT band is also near 500 nm. However, interference between two or more electronic states and/or increasing decomposition of the complex with increasing laser frequency (see section below) may also cause the trend illustrated in Fig. 17.

VI. LASER-INDUCED DISSOCIATION OF VAPORS

It is apparent from the above sections that the feasibility of obtaining spectra from vapors possessing absorption bands in the laser line region, depends on the stability of the molecule at the furnace temperature and on the power and frequency of the excitation line. Following is a more detail examination of the laser line effect on "colored" vapors at elevated temperature. Data on both the dimer-monomer iron(III) chloride and on vapor complexes are presented and discussed.

Iron(III) chloride. Vapor pressure studies[40] have shown that the vaporization of iron(III) chloride yields the monomer-dimer equilibrium:

$$Fe_2Cl_6(g) \rightleftarrows 2FeCl_3(g) \qquad (15)$$

Increasing the temperature results in partial decomposition and the formation of Fe(II):

$$2FeCl_3(g) \rightleftarrows FeCl_2(s) + Cl_2(g) \qquad (16)$$

The vapors formed according to eq. 15 are brown-yellow and the tail of their CT bands extends and covers the laser frequencies.

For obtaining Raman spectra from these vapors, iron trichloride cells with and without excess Cl_2 were used. At temperatures below 620 K the laser beam was quickly blocked by the formation of $FeCl_2(s)$ at the focusing point of entrance into the cell. Rotation of the cell temporarily solved the problem but after 5-10 min a "line" of solid $FeCl_2$ was formed along the periphery of the cell where the beam was focused. With excess $Cl_2(g)$ ($\sim$1 atm) present in the cell and at temperatures near or above 650 K it was possible to reverse reaction 16, evaporate the $FeCl_2(s)$,

unblock the beam, and obtain spectra from the iron(III) chlorides at pressures ~0.02 atm. Figure 18 shows representative spectra of the $FeCl_3$-Fe_2Cl_6 vapor system measured with different excitation lines. Apart from the Cl_2 rotational and vibrational-rotational band contours, the spectra contain a series of bands whose intensities change with excitation line. The three predominant bands are at 420, 370, and 305 cm^{-1}. In accordance with the recent matrix isolation IR and Raman studies,[41] the 420 and 305 cm^{-1} bands are assigned to the ν_1 and ν_2 modes of $Fe_2Cl_6(g)$ while the 370 cm^{-1} bands correspond to the ν_1 mode of $FeCl_3(g)$. Assignments of the remaining weak bands will be the subject of a future publication.[42] From the point of view of the present work, it is important to note that the dimer-monomer intensity ratio decreases with increasing laser frequency. The 595.0 nm spectrum is dominated by the $Fe_2Cl_6(g)$ modes while the 457.9 nm spectrum is mainly due to $FeCl_3(g)$. A comparison of the spectra (Fig. 18) with spectra of pure Cl_2 (~1 atm) obtained in separate cells under the same conditions, permitted measurements of the intensities of the ν_1 modes ($FeCl_3$ and Fe_2Cl_6) relative to each other and to those of Cl_2 at ~560 cm^{-1}. It was found that increasing the laser frequency decreases the amount of dimer in favor of the monomer. It must be emphasized that the monomer CT bands lie at higher energies than the dimer CT bands and thus, on going from the red to the blue lines, the (pre) resonance intensities of Fe_2Cl_6 bands should increase faster than those of $FeCl_3$. The opposite effect is observed in Fig. 18.

The effect of laser power on the spectra also leads to increasing $FeCl_3$ intensities. This is depicted in Fig. 19 for the 514.5 nm line at powers of 1 and 5 W. Thus it appears that both the laser power and frequency effects lead to higher spectroscopic temperature, thereby shifting reaction 15

to the right. Since the furnace temperature remains constant during the measurements, the spectra obtained represent a nonequilibrium situations along the passing laser beam.

Copper(II) chloride complexes. The studies of the Cu-Al-Cl and Cu-In-Cl vapors (sections III and IV) indicate that an increase in temperature dissociates the complexes according to the schemes:

$$CuA_2Cl_8(g) \rightleftarrows CuACl_5(g) + ACl_3(g) \qquad (17)$$

$$CuACl_5(g) \rightleftarrows CuCl_2(g) + ACl_3(g) \qquad (18)$$

where A = Al or In. Reaction 17 characterizes the aluminum complex while reaction 18 occurs for the indium complexes. Figures 20 and 21 illustrate the laser power dependence of the Cu-Al-Cl and Cu-In-Cl systems respectively, at constant furnace temperature. The intensities of $CuAl_2Cl_8$ and Al_2Cl_6 bands diminish at higher laser power (Fig. 20) while the $CuAlCl_5$ and $AlCl_3$ intensities increase. This behavior supports dissociation scheme 17. For the Cu-In-Cl vapors (Fig. 21), the relative intensities of $InCl_3(\nu_1)$ to $Cu\text{-}In\text{-}Cl_5(\nu_{Cu\text{-}Cl_t})$ show that at higher laser power the $CuInCl_5$ decreases in favor of $InCl_3$ and thus supports scheme 18. In separate experiments it was found that the monomer-dimer relative intensities of the colorless aluminum and indium chlorides were independent of the laser power and intensity.

These effects observed show that, at constant furnace temperature, the Raman intensities of the carrier gas cannot be used as internal standard of the cell for calculating the (pre)resonance excitation profiles of the complex bands. Furthermore, since the overlap of laser line and absorption band changes with temperature (*e.g.*, broadening of absorption band), then studies

of the relative Raman intensities at different temperatures cannot be used for estimating the thermodynamics of vapor reactions (*e.g.*, reactions 17, 18).

Uranium(V) chloride complex. The effect of the laser power of the $UCl_5 \cdot AlCl_3$ spectra has been examined and typical results are presented in Fig. 22. Increasing laser power enhances the $\nu_1(AlCl_3)$ band intensity and gives rise to a shoulder band at the lower frequency region of the 362 cm^{-1} band. This indicates a decomposition of the complex according to the scheme:

$$2UCl_5 \cdot AlCl_3(g) \rightarrow U_2Cl_{10}(g) + 2AlCl_3(g) \qquad (19)$$

The rising shoulder band is attributed to the 354 cm^{-1} band of $U_2Cl_{10}(g)$.

It has been suggested[43] that the vapor complexes of the actinides and lanthanides may have potential uses for laser isotope separations and/or construction of high power vapor lasers. The data presented here show that decomposition schemes similar to reactions 17, 18, and 19 play an important role (probably negative) for developing these applications.

VII CONCLUSIONS

From the data and discussions presented above, the following conclusive remarks can be made:

a) Resonance Raman spectroscopy can be used to study vibrational frequencies of some "colored" vapor complexes which exist as a minor component in an equilibrium vapor mixture. On the basis of the measured frequencies and Raman selection rules, the structure of the vapor can be characterized.

b) The appearance of a resonance Raman signal depends on both the position of the change transfer band and the thermodynamic stability of the complex.

It also depends on the relative concentrations of the vapors present and on the laser power and frequency used.

c) Increasing the frequency of the excitation line results in a variation in the resonance Raman intensities and a partial dissociation of the complex. Dissociation also occurs with increasing laser power.

d) As a consequence of the laser-induced dissociation, the relative Raman intensities (*i.e.*, complex *vs.* carrier-gas intensities) depend on the frequency and laser power and represent nonequilibrium situation. Hence, estimations of excitation profiles and calculations of gas phase thermodynamic quantities based on the assumption of equilibrium conditions will be grossly in error.

REFERENCES

1. H. Schäfer, Angew. Chem. Int. Ed. 15, 713 (1976). A review article.
2. A. Anundskås and H. A. Øye, Acta Chem. Scand. Ser A 30, 193 (1976).
3. F. P. Emmenegger, Inorg. Chem. 16, 343 (1977).
4. N. W. Gregory, J. Phys. Chem. 81, 1857 (1977).
5. G. N. Papatheodorou and G. H. Kucera, Inorg. Chem. 16, 1006 (1977).
6. E. W. Dewing, Metall. Trans. 1, 2169 (1970).
7. G. N. Papatheodorou, J. Phys. Chem. 77, 472 (1973).
8. G. N. Papatheodorou, Inorg. Chem. 12, 1899 (1973).
9. G. N. Papatheororou, Allgem. Chem. 411, 153 (1975).
10. A. Dell Anna and T. P. Emmenegger, Helv. Chim. Acta 48, 1145 (1975).
11. Von Meinhart and H. Schäefer, Z. Anorg. Allgen. Chem. 408, 37 (1974).
12. A. Anundskås, A. E. Mahyoub and H. A. Øye, Acta Chem. Scand. A30, 193 (1976).
13. F. Dienstbach and E. P. Emmenegger, Helv. Chim. Acta 58, 1145 (1977).
14. G. H. Kucera and G. N. Papatheodorou, to be published (see Abstracts of Papers. American Chemical Society, 174th Meeting; August 28-September 2, 1977).
15. M. A. Capote, G. H. Kucera and G. N. Papatheodorou, in "High Temperature Metal Halide Chemistry," 78-1, 367 (1978) Eds. D. Cubicciotti and D. D. Hildenbrand.
16. I. R. Beattie and J. Horder, J. Chem. Soc. (A) 1969, 2655.
17. B. B. Johnson and W. L. Peticolas, Ann. Rev. Phys. Chem. 27, 465 (1976).
18. G. N. Papatheodorou and G. H. Kucera, Inorg. Chem. (submitted).
19. G. N. Papatheodorou, J. Chem. Phys. 66, 2893 (1977).
20. M. Sørlie and H. A. Øye, Inorg. Chem. (in press).
21. G. N. Papatheodorou, unpublished results.

22. S. Sutakshuto, "Copper(II) Chloride Gas Complexation With Acid Halides," Thesis No. 31, Institute of Inorganic Chemistry, University of Trondheim (1976).

23. G. N. Papatheodorou and M. A. Capote, J. Chem. Phys. 69 xxx (1978).

24. M. A. Capote and G. N. Papatheodorou, Inorg. Chem. (submitted).

25. Y. M. Bosworth and R. J. H. Clark, Inorg. Chem. 14, 170 (1975).

26. P. Stein, V. Miskowski, W. H. Woodruff, J. P. Griffen, K. G. Werner, B. P. Gaber and T. G. Spiro, J. Chem. Phys. 64, 2159 (1976).

27. R. J. H. Clark and W. R. Truble, Inorg. Chem. 15, 1030 (1976).

28. M. Z. Zgierski, J. Raman Spectrosc. 6, 53 (1977).

29. The effect of nearest-neighbor cations (Li^+, K^+, Cs^+, Al^{+3}) on the electronic states of $PtCl_4^{-2}$ has been investigated and showed that energy shifts of ∿2 to 3 kK occur in the excited states $^1A_{2g}$ and ^1E_g of Pt(II) by substituting low field ions (*i.e.*, Cs^+) with high field ions (*i.e.*, Li^+). See *e.g.*, G. N. Papatheodorou and G. P. Smith, J. Inorg. Nucl. Chem. 35, 799 (1973), and Ref. 8.

30. G. Chottard and J. Bolard, Chem. Phys. Let. 33, 309 (1975).

31. R. M. Rush, D. S. Martin and R. G. LeGrand, Inorg. Chem., 14, 2543 (1975).

32. J. J. Avery, C. D. Burbridge and D. L. Goodgame, Spectrochim. Acta 24A, 1721 (1968).

33. C. W. Schläpfer and C. Rohrbasser, Inorg. Chem. 17, 1623 (1978).

34. G. E. Leroi, T. C. Jones, J. T. Hougen and W. Klemperer, J. Chem. Phys. 36, 2879 (1962).

35. D. M. Gruen, J. R. Clifton and C. W. DeKock, J. Chem. Phys. 48, 1394 (1968).

36. J. R. Ferraro, "Low Frequency Vibrations of Inorganic and Coordination Compounds" Plenum Press, New York, 1971, p. 140.

37. F. Dienstbach and F. P. Emmenegger, Z. Anorg. Allg. Chem. 436, 127 (1977).

38. D. M. Gruen and R. L. McBeth, Inorg. Chem. 8, 2625 (1969).

39. D. L. Hildenbrand and D. D. Cubicciotti, Stanford Research Institute Report, UCRL-13657 (1975).

40. C. F. Shieh and N. W. Gregory, J. Phys. Chem. 79, 828 (1975), and references therein.

41. A. Loewenschuss and A. Givan, Ber. Bunsenges. Phys. Chem. 82, 74 (1978).

42. G. N. Papatheodorou, to be submitted for publication.

43. R. R. Jacobs and W. F. Krupke; in Lawrence Livermore Laboratory report, UCRL-50021-75 (1976), p. 529.

Table I

Aluminum Halide-Transition Metal(II) Halide Vapors
Investigated by Raman Spectroscopy

System	Predominant Vapor Complex	Reference for Absorption Spectra	Observed Raman Bands
Ti-Al-Cl	$TiAl_3Cl_{11}$ (20)	20	Acidic vapor bands only
Fe-Al-Cl	$FeAl_2Cl_8$ (6)	21	>>
Co-Al-Cl	$CoAl_2Cl_8$ (6)(9)	9	>>
Co-Al-Br	$CoAl_2Br_8$ (5)	5	>>
Cu-Al-Cl	$CuAl_2Cl_8$ (22)	22,23	Bands due to $CuAl_2Cl_8$, $CuAlCl_5$ and Al_2Cl_6-$AlCl_3$
Ni-Al-Cl	$NiAl_2Cl_8$ (6)	7	Acidic vapor bands only
Pd-Al-Cl	$PdAl_2Cl_8$ (7)	7	Bands due to $PdAl_2Cl_8$ and Al_2Cl_6-$AlCl_3$
Pd-Al-Br	$PdAl_2Br_8$ (15)	15,24	Bands due to $PdAl_2Br_8$ and Al_2Br_6-$AlBr_3$
Pt-Al-Cl	$PtAl_2Cl_8$ (8)	8	Acidic vapor bands only

Table II

Resonance Raman Bands Attributed to Gaseous MA_2X_8 Molecules (Frequency in cm^{-1})

Band	$PdAl_2Cl_8$	$PdAl_2Br_6$	$CuAl_2Cl_6$	Assignment
I	84.5	59	84.5	$\nu_{ring\ def.}$
II	176	114	174.5	$\delta_{MX_{2b}}$
III	298	180	281	ν_{M-X_b}

Table III

Resonance Raman Bands Attributed to Gaseous $CuACl_5$ and Cu_2Cl_4 Molecules (Frequency in cm^{-1})

Band	$CuAlCl_5$	$CuInCl_5$	Cu_2Cl_4	Assignment
I	291	300	314	ν_{Cu-Cl_b}
II	448	442	442	ν_{Cu-Cl_t}

Table IV

Observed Frequencies (cm^{-1}) of MX_2 Vapors at Elevated Temperatures

	$FeCl_2$	$CoCl_2$	$NiCl_2$	$CuCl_2$	$ZnCl_2$
Temperature K	1100	1100	900	800	975
ν_1	350 p	359	362	370 p	362 p
ν_2		177(?)[a]	170(?)[a]	130 p	
ν_3				503 dp	
Molecular Symmetry	$D_{\infty h}$	$D_{\infty h}$(?)	$D_{\infty h}$(?)	C_{2v}	$D_{\infty h}$

[a]Tentative assignment.

FIGURE CAPTIONS

Fig. 1. Instrumentation for High Temperature Raman Spectroscopy. The distance between the furnace and entrance slit is ∿50 cm.

Fig. 2. Optical Furnace

A: Lavite Rings, B: Main Inconel Heater

C: Bubble Alumina Insulation

D: Inconel Tube Opening, E: Inconel Conical Opening

F: Fused Silica Windows, G: Water Cooling

H: Brass Supports, I: Controlling Thermocouple

J: Measuring Thermocouple, K: Lavite Plugs.

Fig. 3. Electronic Absorption Spectra of nd^8 Vapor Complexes $NiAl_2Cl_8$;[7] $PdAl_2Cl_8$;[7] $PtAl_2Cl_8$.[8,21] Vertical lines define the 647.1 to 457.9 nm region of laser frequencies. —.—.—, calculated excitation profile (1 kK = 1000 cm^{-1}).

Fig. 4. Raman Spectrum of Gaseous $PdAl_2Cl_8$-Al_2Cl_6 Mixture.

$P_{Al_2Cl_6}$ ∿1 atm; excess of $PdCl_2$(s), λ_o = 647.1 nm; laser power 900 mW. Spectral slit width, ∿6 cm^{-1}; scan speed, 0.22 nm/min; time constant, 3 sec; polarization: upper spectrum $\perp$, $\perp$; lower spectrum $\parallel$, $\perp$; a, c, d are the bands attributed to the gaseous complex.

Fig. 5. Raman Spectrum of $PdAl_2Br_8$-Al_2Br_6-$AlBr_3$ Vapor Mixture.

$P_{Al_2Br_6}$ ∿1 atm, no $PdBr_2$ excess; λ_o = 488.0 nm; laser power 1W; spectral slit width, ∿6 cm^{-1}; scan speed 4 nm/min; time constant, 0.6 sec; polarization $\perp$, $\perp$.

Fig. 6. Molecular Models for MA_2X_8 Vapors with M as Central Atom.

Symmetries: a = D_{3h}; b = D_{2h}; c = D_{2d}.

Fig. 7. Raman Spectra of Cu-Al-Cl Vapor Complexes. $P_{Al_2Cl_6}$ ~0.3 atm; furnace temperature, ~575 K; spectral slit width, ~7 cm^{-1}; polarization $\perp$, $\perp$. Note that the spectra were obtained using a double monochromator linear in wavelength and that the abscissa should be used only for approximating the band positions.

Fig. 8. Effect of Aluminum Chloride Pressure on Raman Intensity of the 448 cm^{-1} Band. Furnace temperature, 625 K; power, 500 mW; spectral slit width, ~8 cm^{-1}. Numbers in parentheses indicate the intensity in counts/sec.

Fig. 9. Molecular Models for MAX_5 and M_2X_4 Vapors.

Fig. 10. Raman Spectra of Vapors over Liquid $ZnCl_2$. Spectral slit width; ~4 cm^{-1}; power, 6 W; scan speed, 20 cm^{-1}/min; time constant, 0.5 sec.

Fig. 11. Temperature dependence of copper chloride spectra. No $CuCl_2$(s) excess; spectral slit width, ~7.5 cm^{-1}; power, 740 mW; polarization $\perp$,$\perp$, scan speed, 2.2 Å/min; time constant, 1.5 sec;
* = fluorescence bands.

Fig. 12. Nickel Chloride Vapor Spectrum Excited with 457.9 nm Laser Line. Spectral slit width, ~4.5 cm^{-1}; power, 250 mW; scan speed, 500 cm^{-1}/min; time constant, 0.2 sec.

Fig. 13, Spectra of Cu-In-Cl Vapors. Spectral slit width , ~7.5 cm^{-1}; power, 750 mW; polarizations $\perp$,$\perp$ and $\parallel$,$\perp$; scan speed, 6 Å/min; time constant, 1 sec.

Fig. 14. Temperature Dependence of the Cu-In-Cl Spectra. No $CuCl_2$(s) excess ; spectral slit width, ~7.5 cm^{-1}; power, 750 mW; polarization $\perp$, $\perp$; scan speed , 6 Å/min; time constants, 0.5 to 1.2 sec;
* = fluorescence bands.

Fig. 15. Raman Spectra of $U_2Cl_{10}(g)$ and $UCl_5 \cdot AlCl_3(g)$ in the Presence of $Cl_2(g)$ at 500 K Excited with the 514.5 nm Line. $U_2Cl_{10}(g)$: spectral slit width, 7.5 cm^{-1}; power, 6 W; scan speed, 10 cm^{-1}/min; time constant, 1 sec. $UCl_3 \cdot AlCl_3(g)$; spectral slit width, 6 cm^{-1}; power, 2 W; scan speed, 20 cm^{-1}/min; time constant, 0.25 sec.

Fig. 16. Molecular models for U_2Cl_{10} and $UCl_5 \cdot AlCl_3$ vapors.

Fig. 17. Dependence of the U(V)-Al-Cl spectra on excitation line. Intensity 1 watt; spectral slit width, 6 cm^{-1}; temp. 500 K. The 5017 Å scan was at 10 cm^{-1}/min; time constant of 1 sec. The 4579 Å scan was at 2 cm^{-1}/min; time constant of 3 sec.

Fig. 18. Raman Spectra of Fe_2Cl_6-$FeCl_3$-Cl_2 Vapors. Polarization $\perp$; $\perp$. λ_o = 595.0 nm: slit width, ~7 cm^{-1}; time constant, 1 sec; power, 700 mW; scan speed, 20 cm^{-1}/min. λ_o = 514.5 nm: slit width, 7.5 cm^{-1}; time constant, 0.8 sec; power, 1 W; scan speed, 20 cm^{-1}/min. λ_o = 457.9 nm: slit width, 7.5 cm^{-1}; time constant, 0.5 sec; power, 1 W; scan speed, 20 cm^{-1}/min.

Fig. 19. Effect of the Intensity of Excitation Line on the Raman Spectra of the Fe_2Cl_6-$FeCl_3$ Vapors. Polarization $\perp$, $\perp$; slit width, ~7.5 cm^{-1}; time constant, 0.25 sec; scan speed, 20 cm^{-1}/min.

Fig. 20. Effect of the Intensity of Excitation Line on the Raman Spectra of the Cu-Al-Cl Gaseous Complexes. $P_{Al_2Cl_6}$, ~0.3 atm; spectral slit width, ~8 cm^{-1}; polarization $\perp$, $\perp$.

Fig. 21. Dependence of the Cu-In-Cl spectra on laser line intensity. Polarization $\perp$, $\perp$; slit width, 7.5 cm^{-1}; time constants, 1 to 1.25 sec; scan speed, 6 Å/min.

Fig. 22. Dependence of the U(V)-Al-Cl Spectra on Laser Line Intensity. Excitation line 4880 nm; scan speed, 10 cm^{-1}/min; time constant, 1 sec; slit width, 6 cm^{-1}.

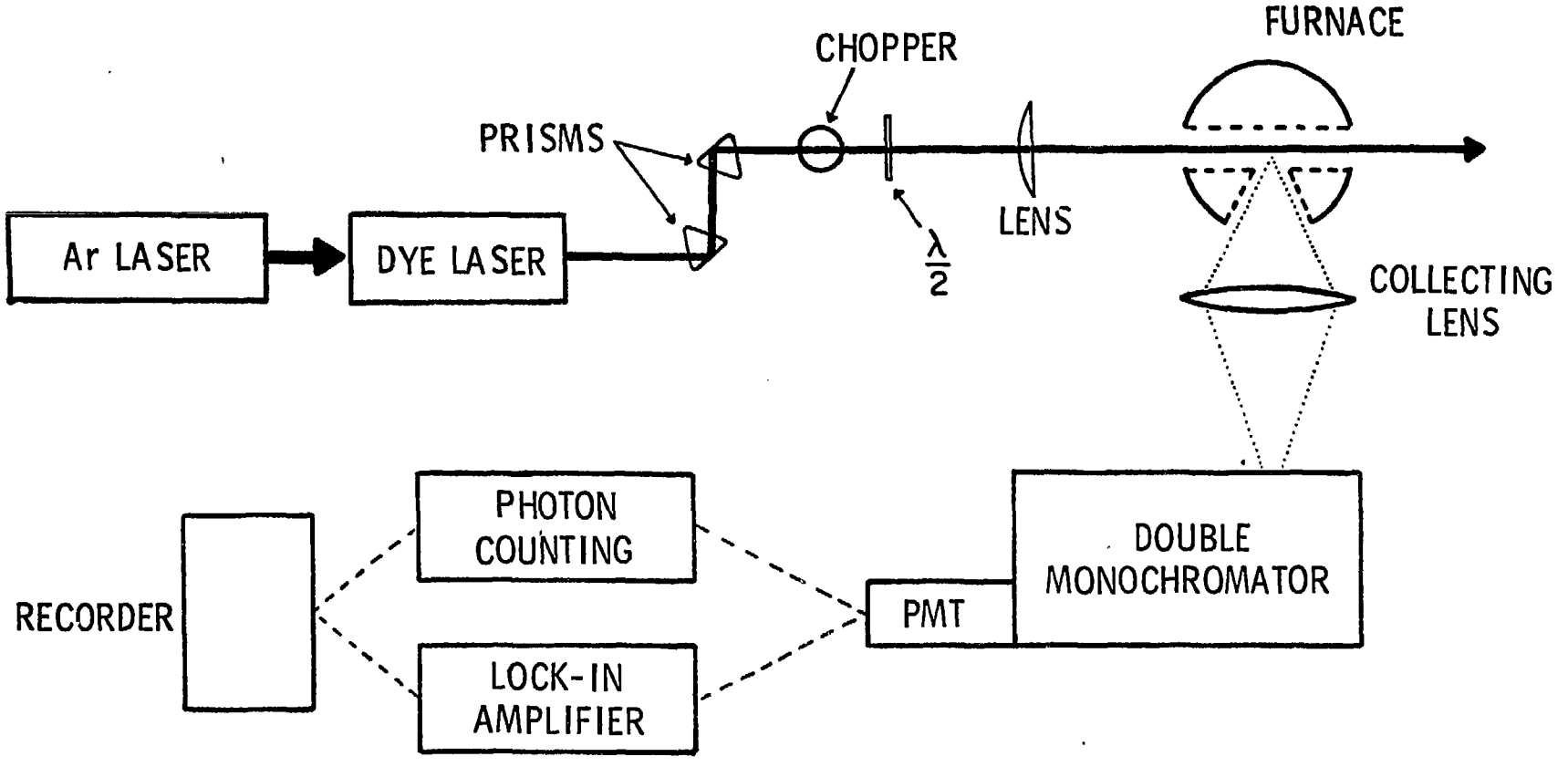
FURNACE
CHOPPER
PRISMS
LENS
Ar LASER
DYE LASER
λ/2
COLLECTING LENS
PHOTON COUNTING
DOUBLE MONOCHROMATOR
RECORDER
PMT
LOCK-IN AMPLIFIER

Fig. 1

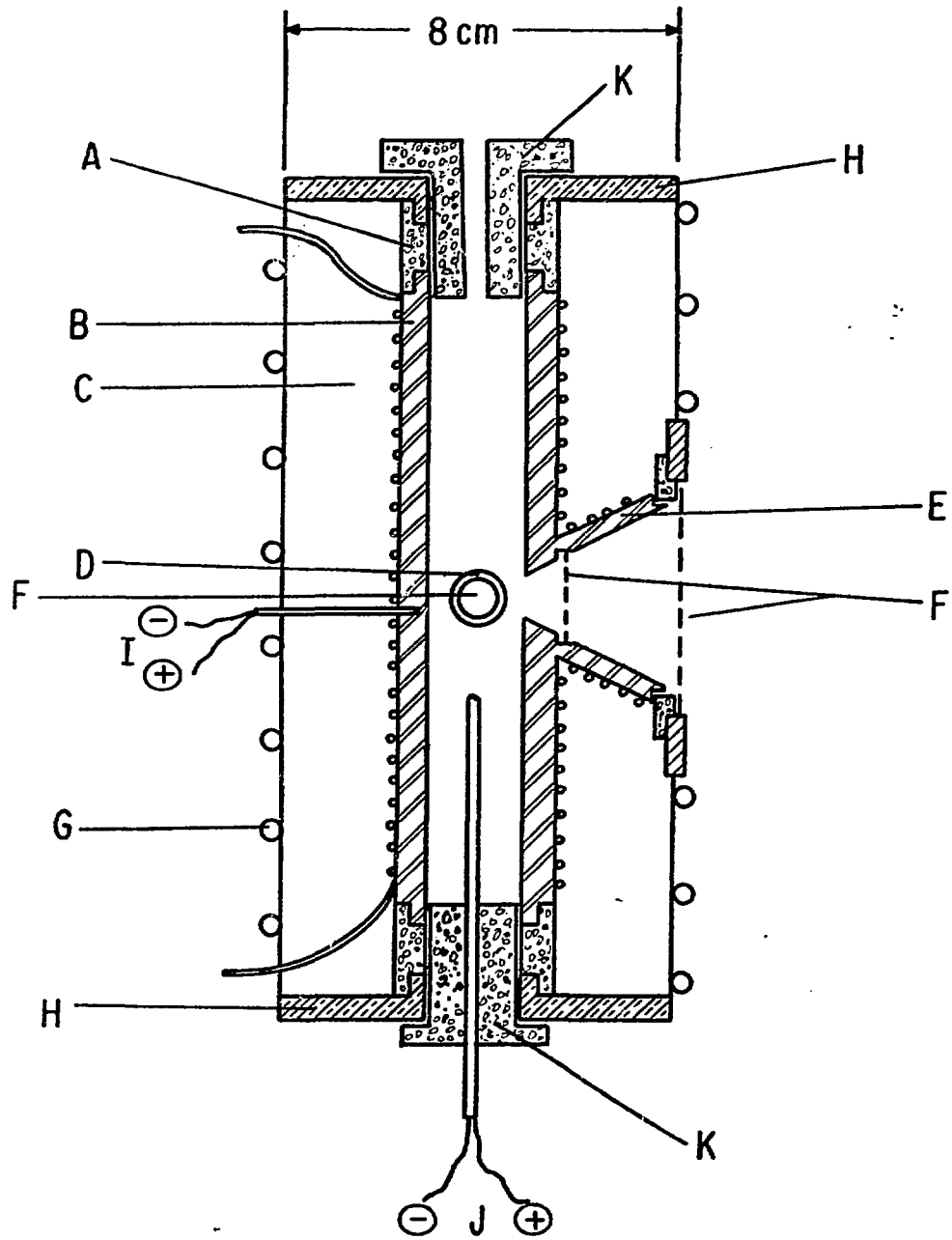

Fig. 2

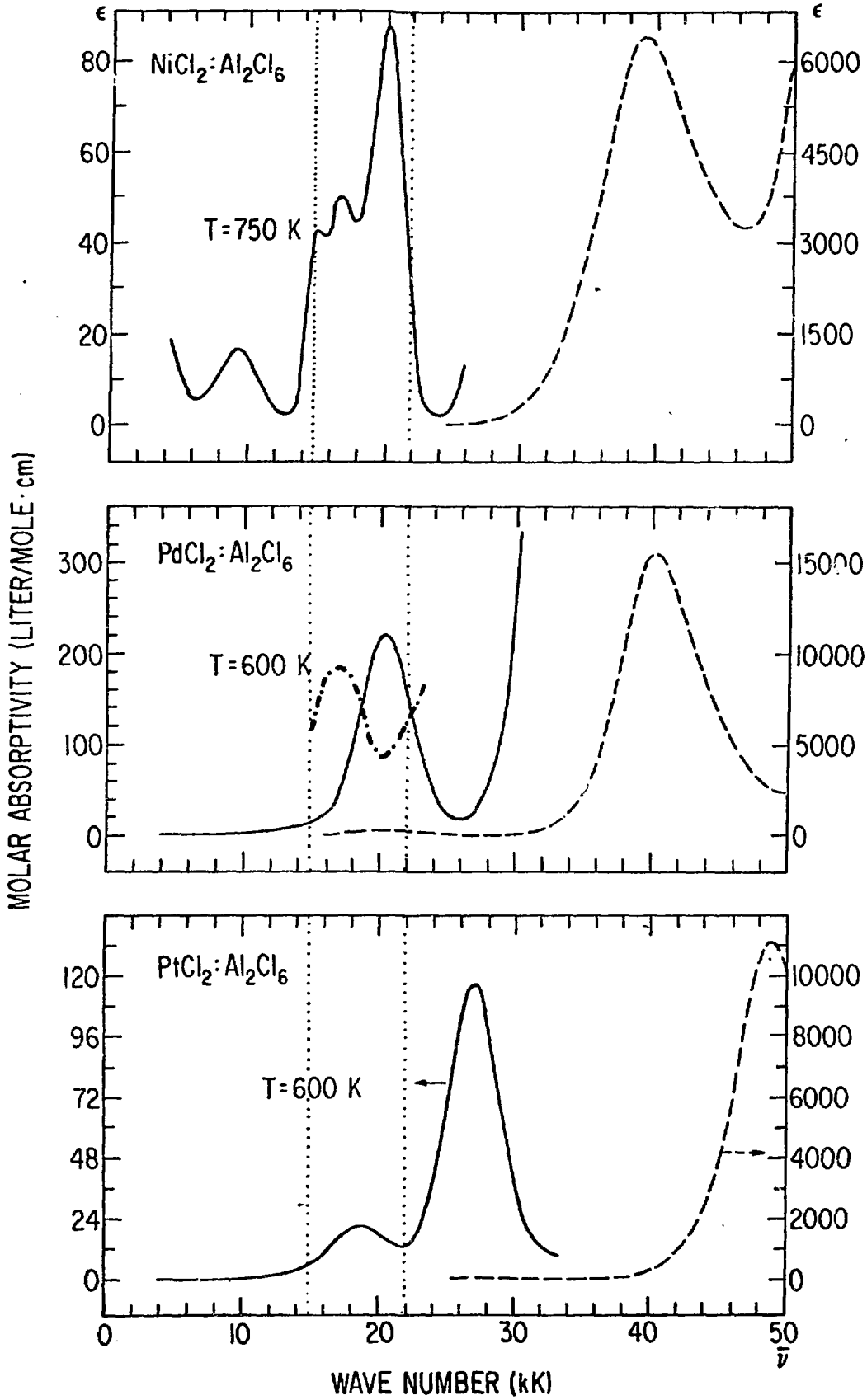
ε
80
60
40
20
0
NiCl2:Al2Cl6
T=750 K
ε
6000
4500
3000
1500
0
300
200
100
0
PdCl2:Al2Cl6
T=600 K
15000
10000
5000
0
120
96
72
48
24
0
PtCl2:Al2Cl6
T=600 K
10000
8000
6000
4000
2000
0
0
10
20
30
40
50
ν̄
WAVE NUMBER (kK)
MOLAR ABSORPTIVITY (LITER/MOLE·cm)

Fig. 3

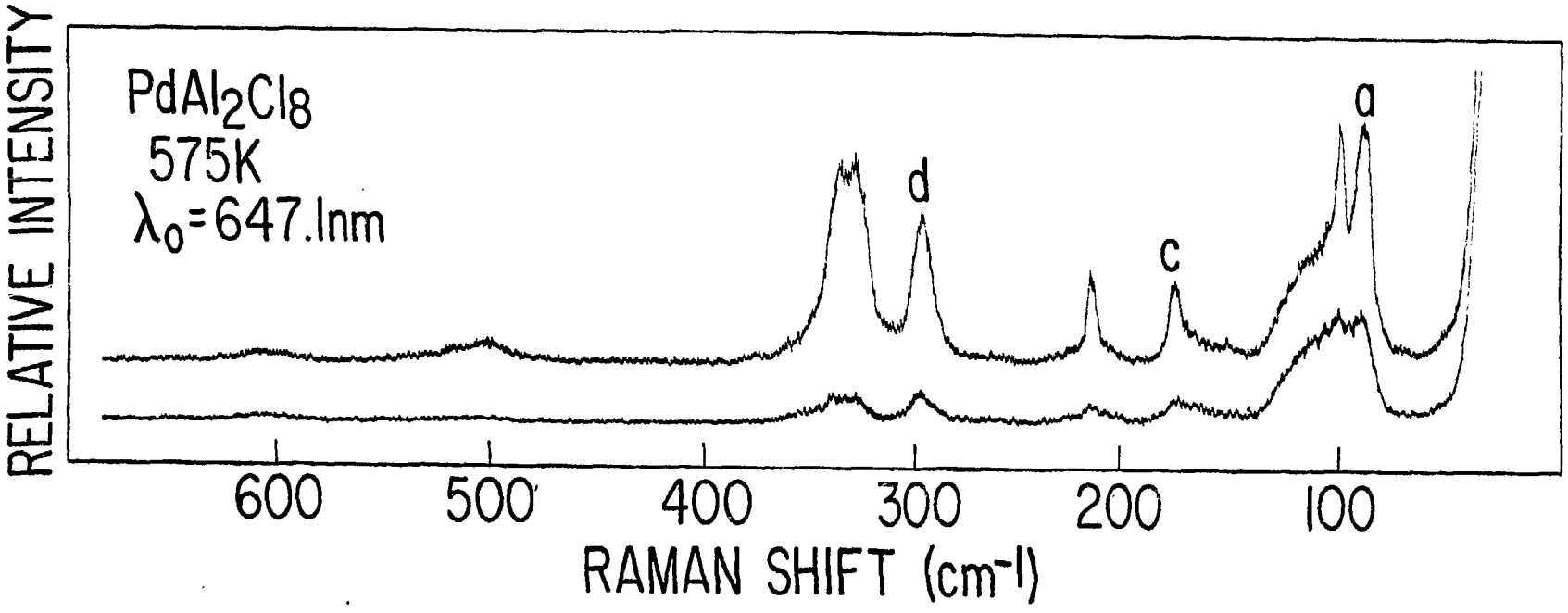
RELATIVE INTENSITY
PdAl2Cl8
575K
λ0=647.1nm
d
c
a
600
500
400
300
200
100
RAMAN SHIFT (cm-1)

Fig. 4

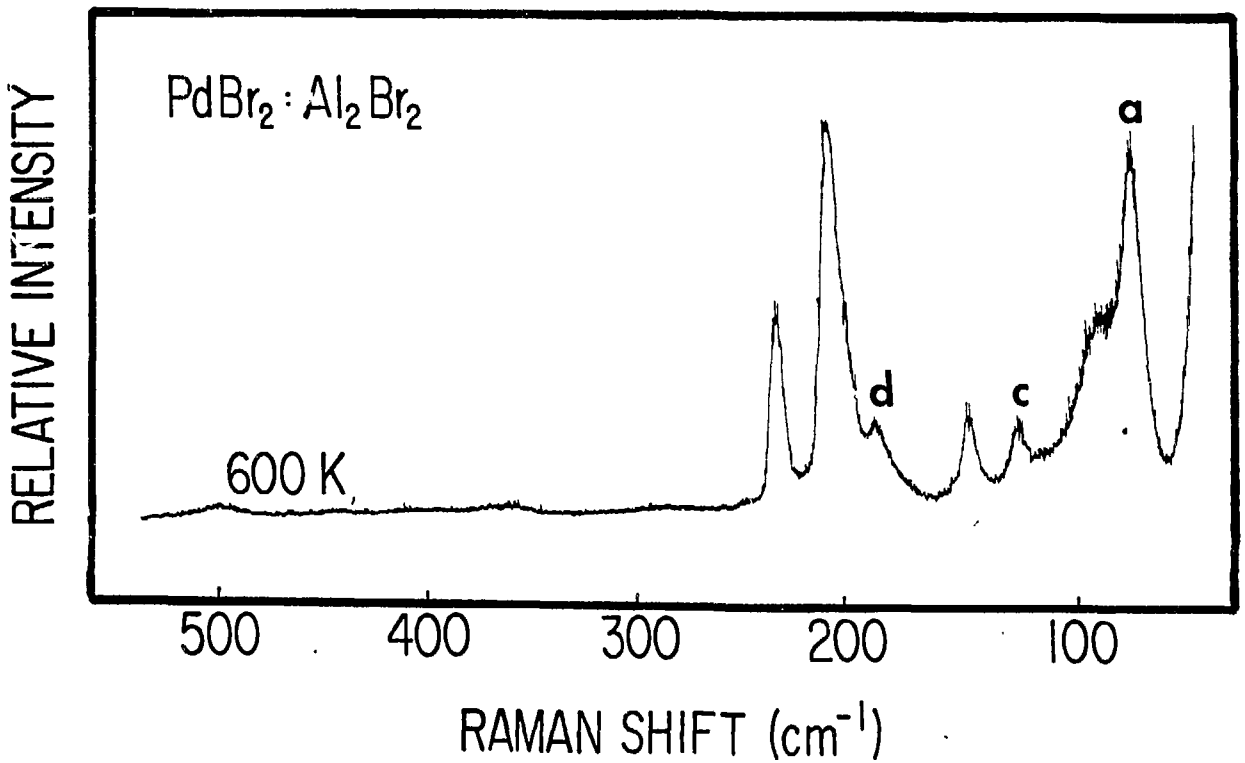
PdBr2 : Al2 Br2
a
d
c
600 K
RELATIVE INTENSITY
500
400
300
200
100
RAMAN SHIFT (cm-1)

Fig. 5

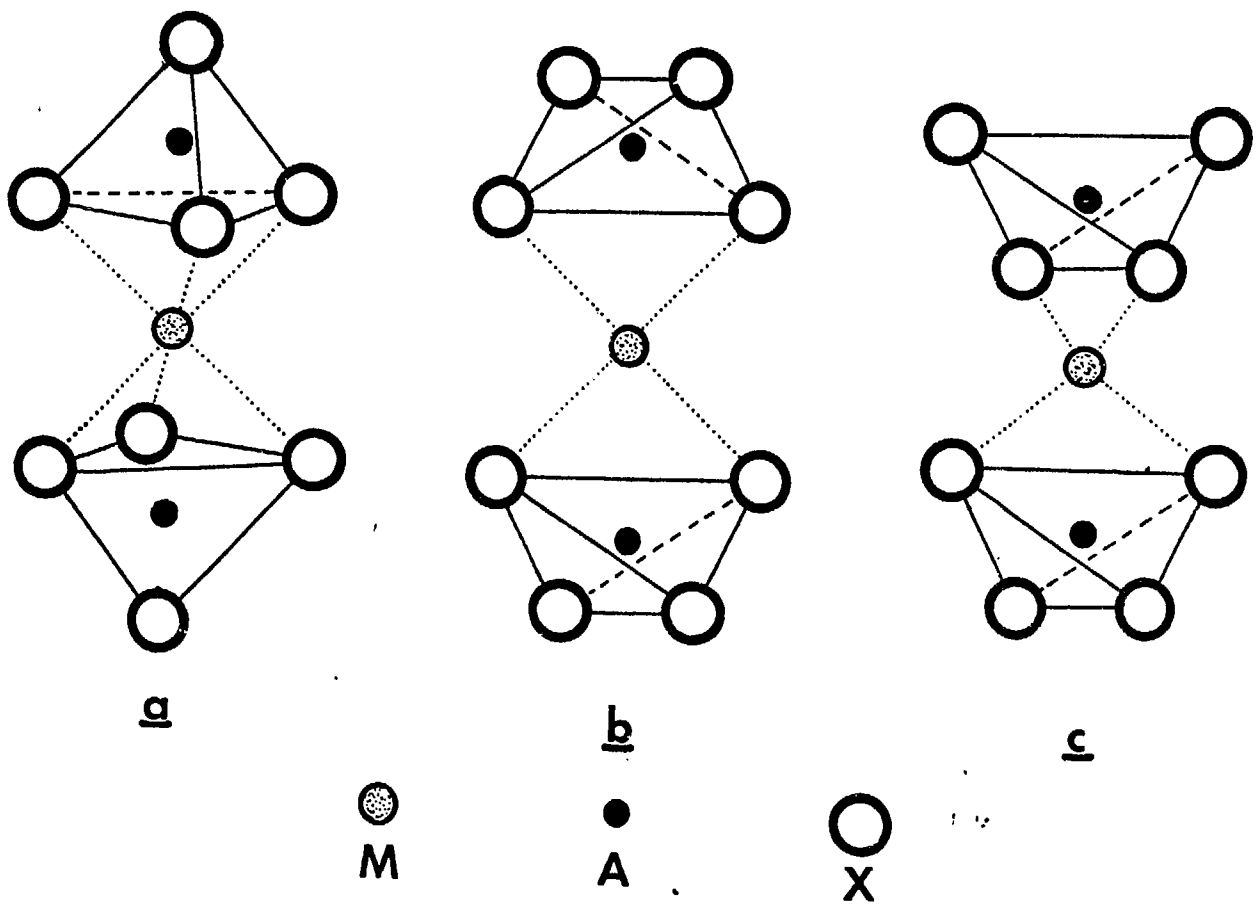

Fig. 6

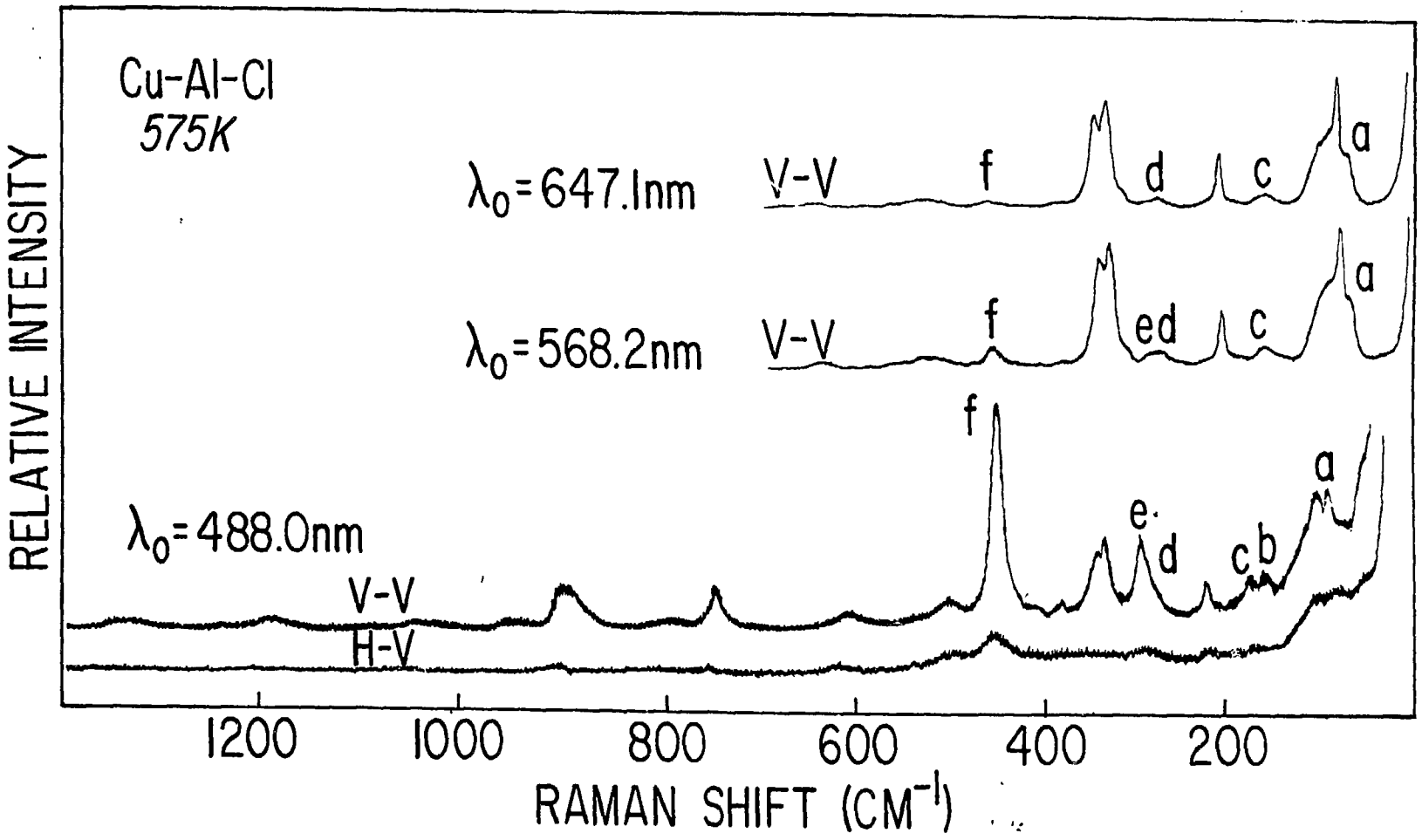
Cu-Al-Cl
575K
λ0=647.1nm
V-V
f
d
c
a
λ0=568.2nm
V-V
f
ed
c
a
λ0=488.0nm
V-V
H-V
f
e
d
c
b
a
RELATIVE INTENSITY
1200
1000
800
600
400
200
RAMAN SHIFT (CM-1)

Fig. 7

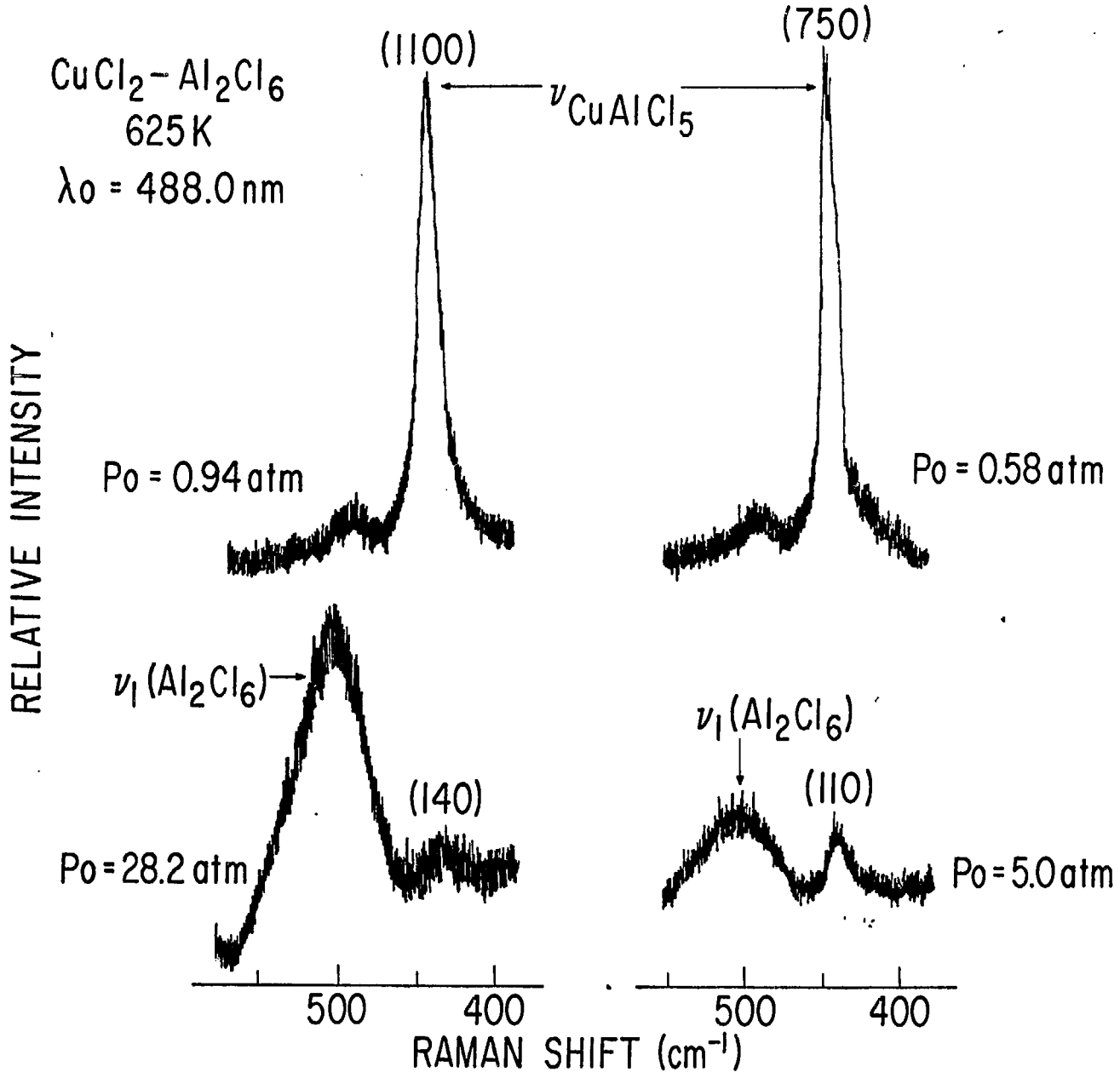
$CuCl_2 - Al_2Cl_6$
625 K
λo = 488.0 nm
(1100)
ν_{CuAlCl_5}
(750)
RELATIVE INTENSITY
Po = 0.94 atm
Po = 0.58 atm
$\nu_1 (Al_2Cl_6)$
(140)
Po = 28.2 atm
$\nu_1 (Al_2Cl_6)$
(110)
Po = 5.0 atm
500
400
500
400
RAMAN SHIFT (cm^{-1})

Fig. 8

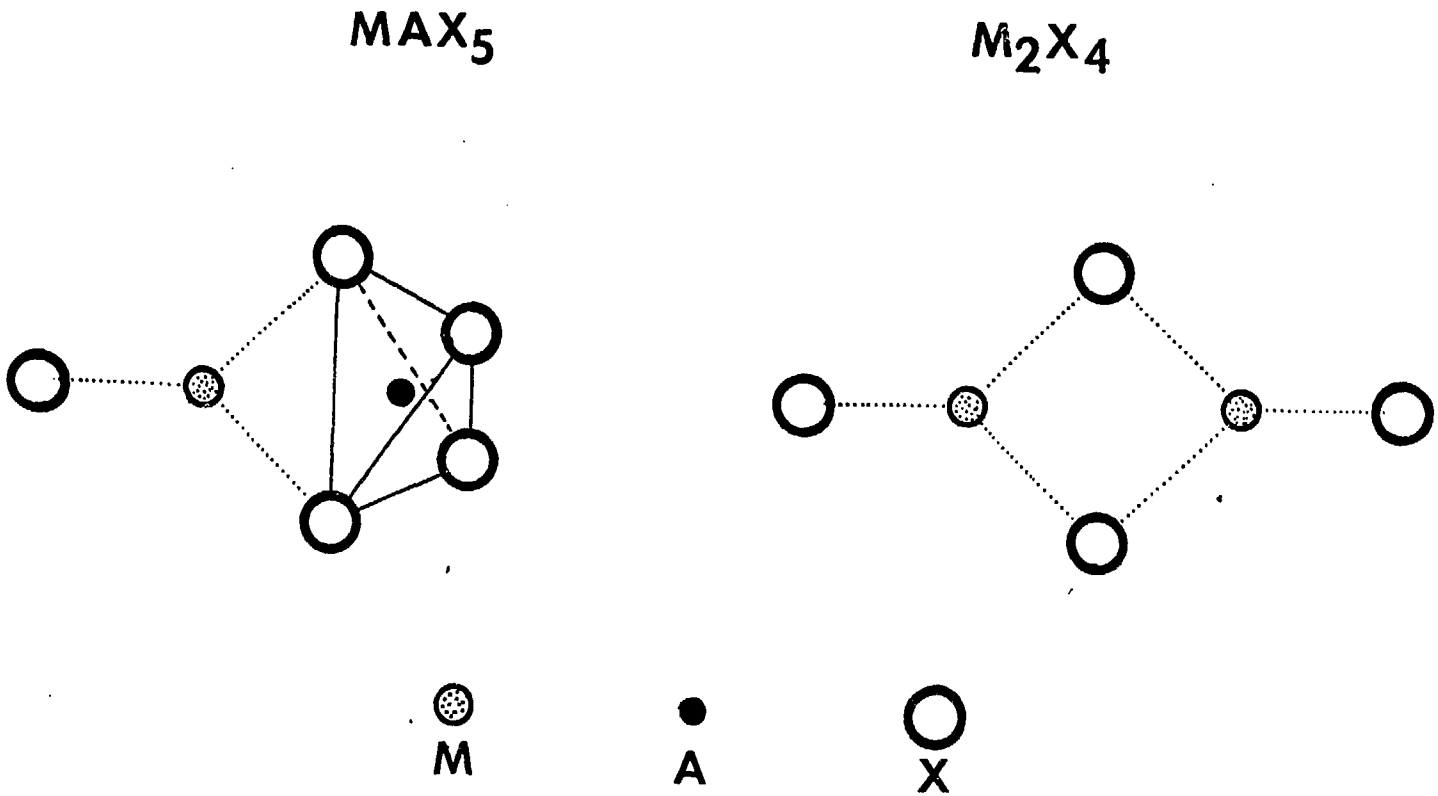

Fig. 9

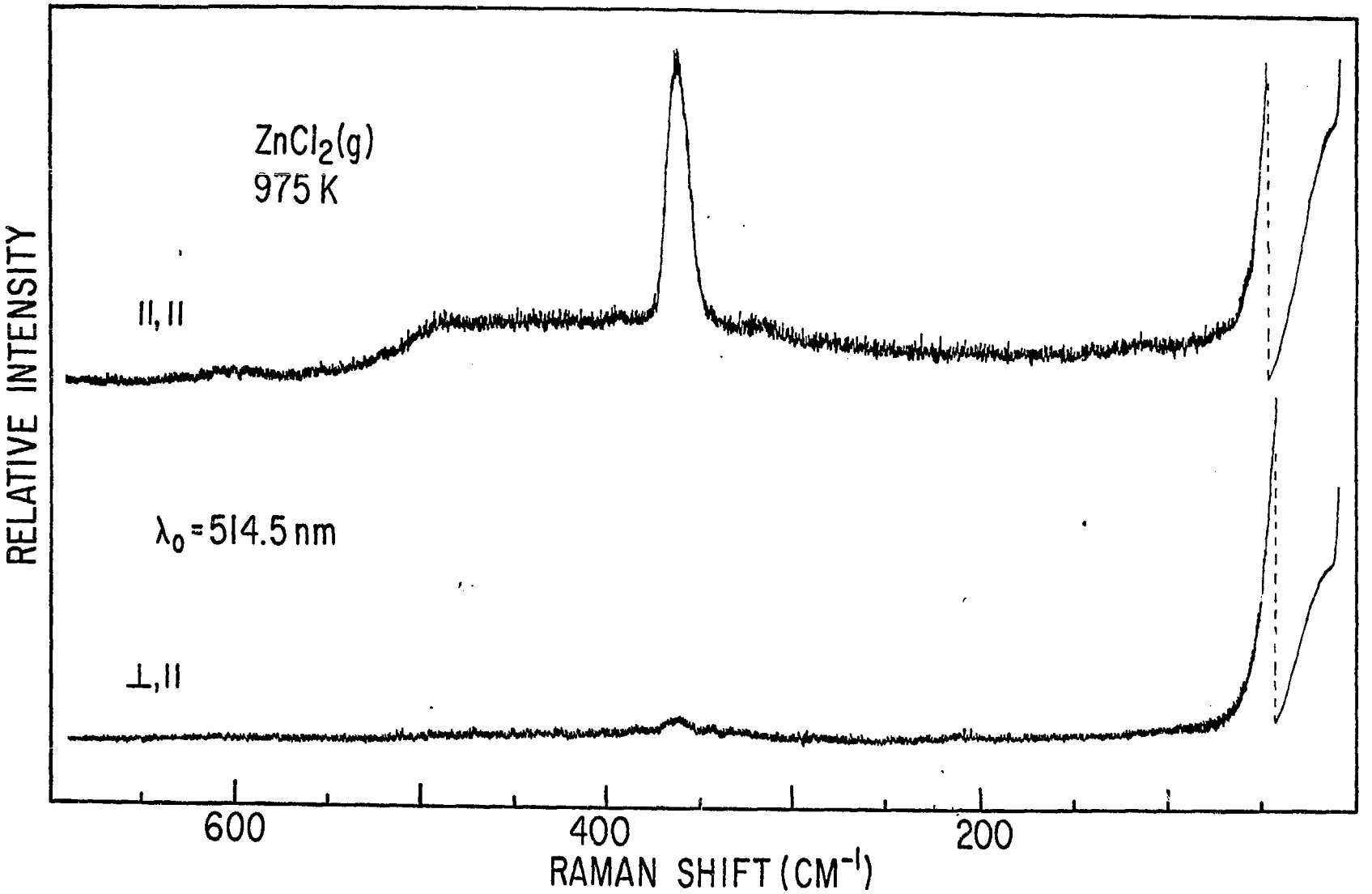
$ZnCl_2(g)$
975 K
II, II
$\lambda_0 = 514.5$ nm
⊥, II
RELATIVE INTENSITY
600
400
200
RAMAN SHIFT (CM^{-1})

Fig. 10

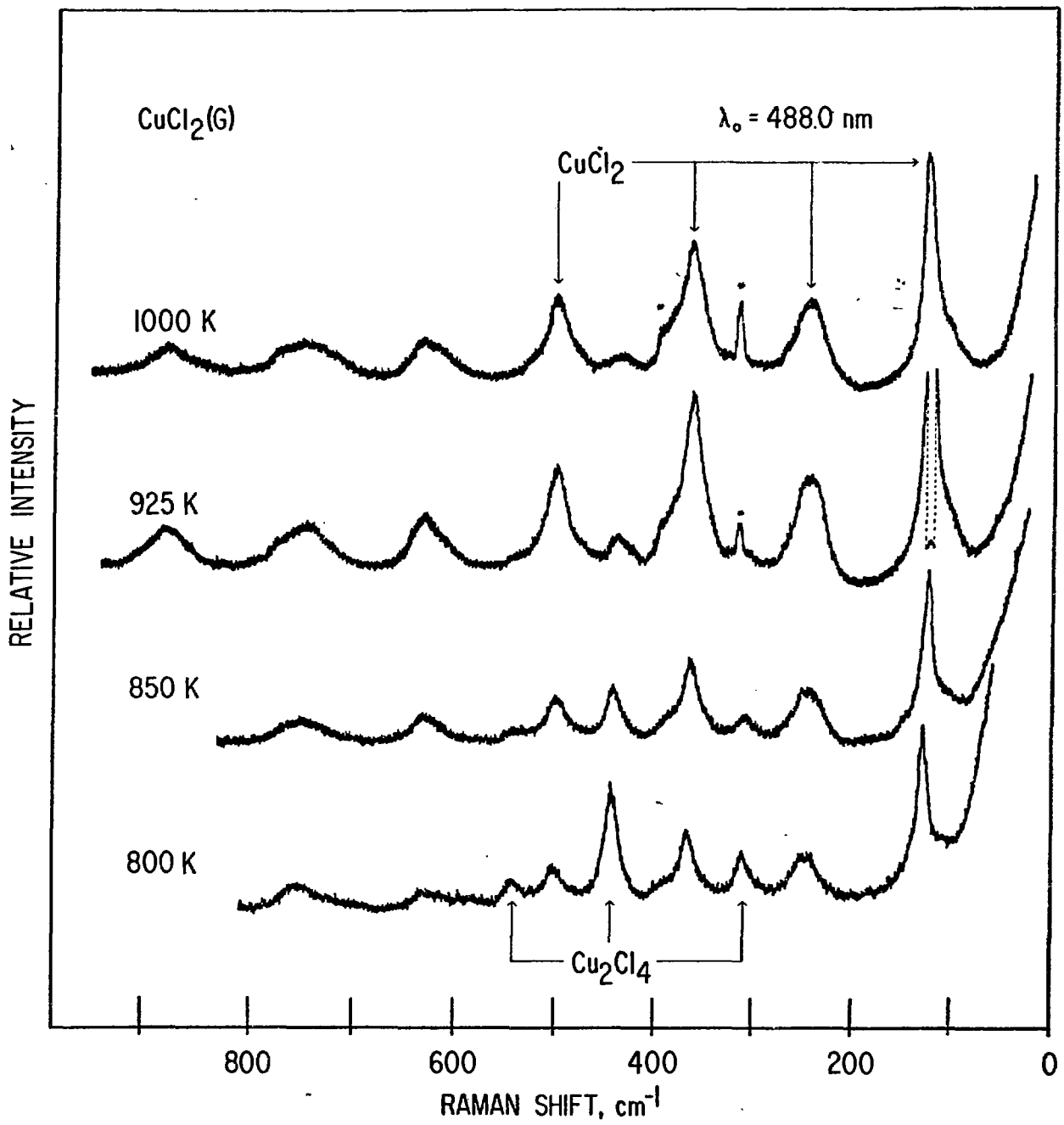
CuCl2(G)
λo = 488.0 nm
CuCl2
1000 K
925 K
850 K
800 K
Cu2Cl4
RELATIVE INTENSITY
800
600
400
200
0
RAMAN SHIFT, cm-1

Fig. 11

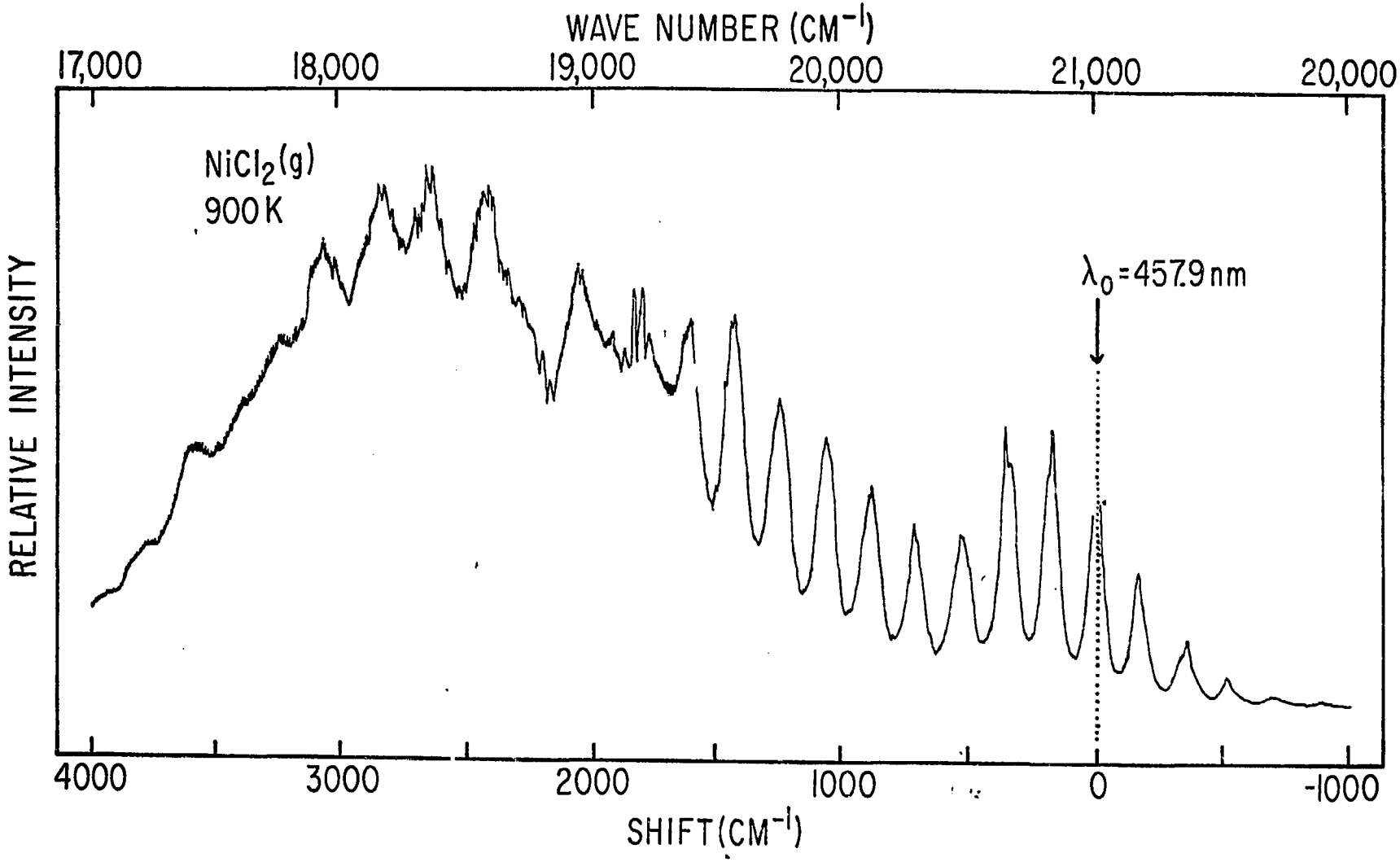
WAVE NUMBER (CM⁻¹)
17,000
18,000
19,000
20,000
21,000
20,000
NiCl2(g)
900 K
λ0 = 457.9 nm
RELATIVE INTENSITY
4000
3000
2000
1000
0
-1000
SHIFT (CM⁻¹)

Fig. 12

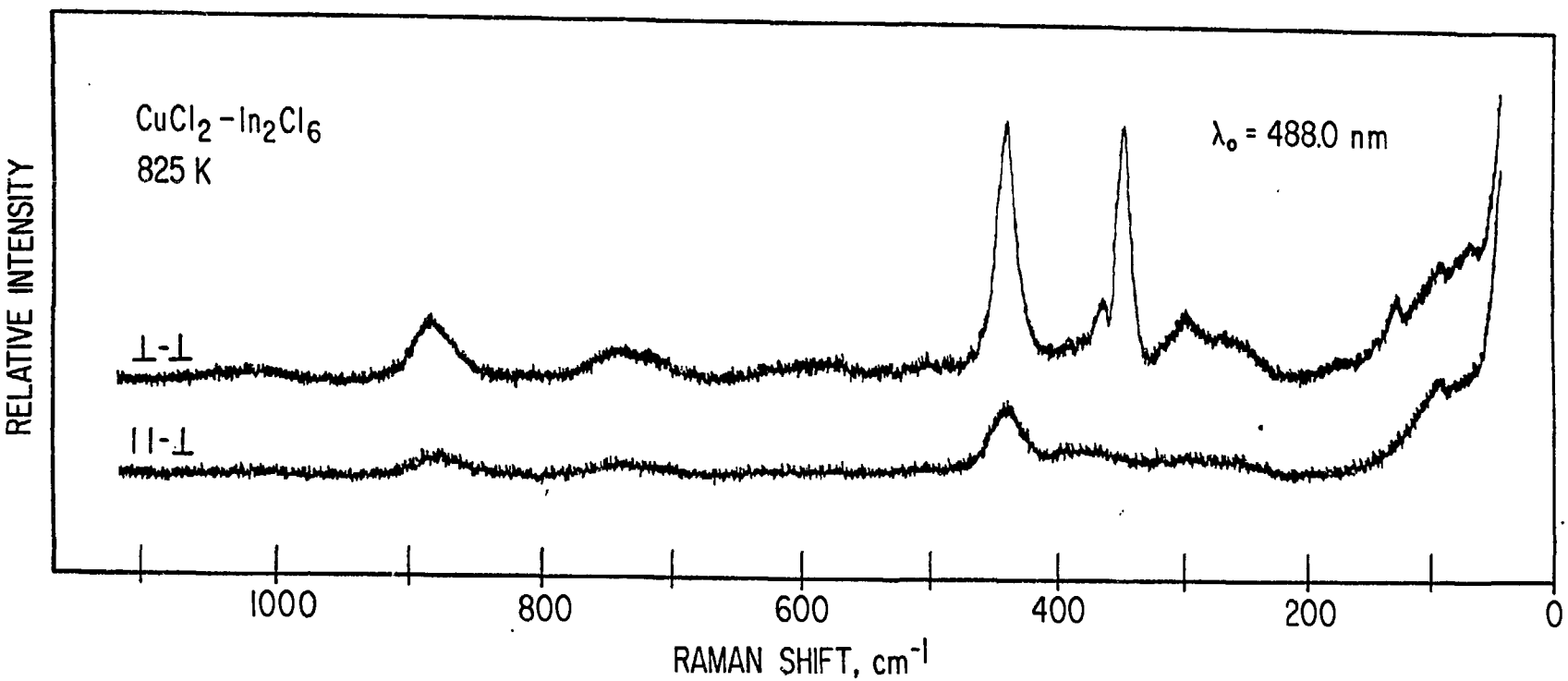
$CuCl_2 - In_2Cl_6$
825 K
λ_o = 488.0 nm
⊥-⊥
∥-⊥
RELATIVE INTENSITY
1000
800
600
400
200
0
RAMAN SHIFT, cm^{-1}

Fig. 13

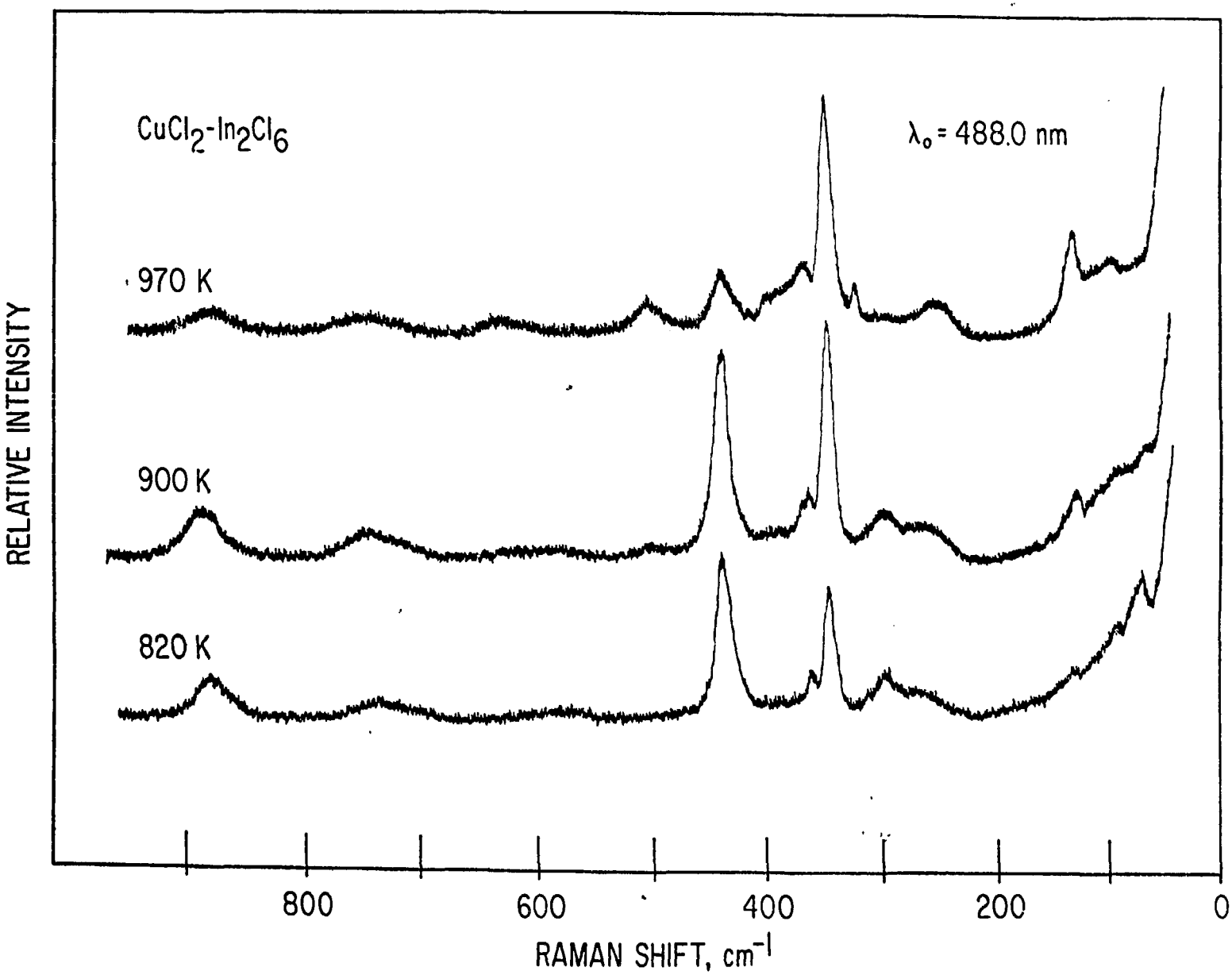
$CuCl_2$-In_2Cl_6
λ_o = 488.0 nm
970 K
900 K
820 K
RELATIVE INTENSITY
800
600
400
200
0
RAMAN SHIFT, cm^{-1}

Fig. 14

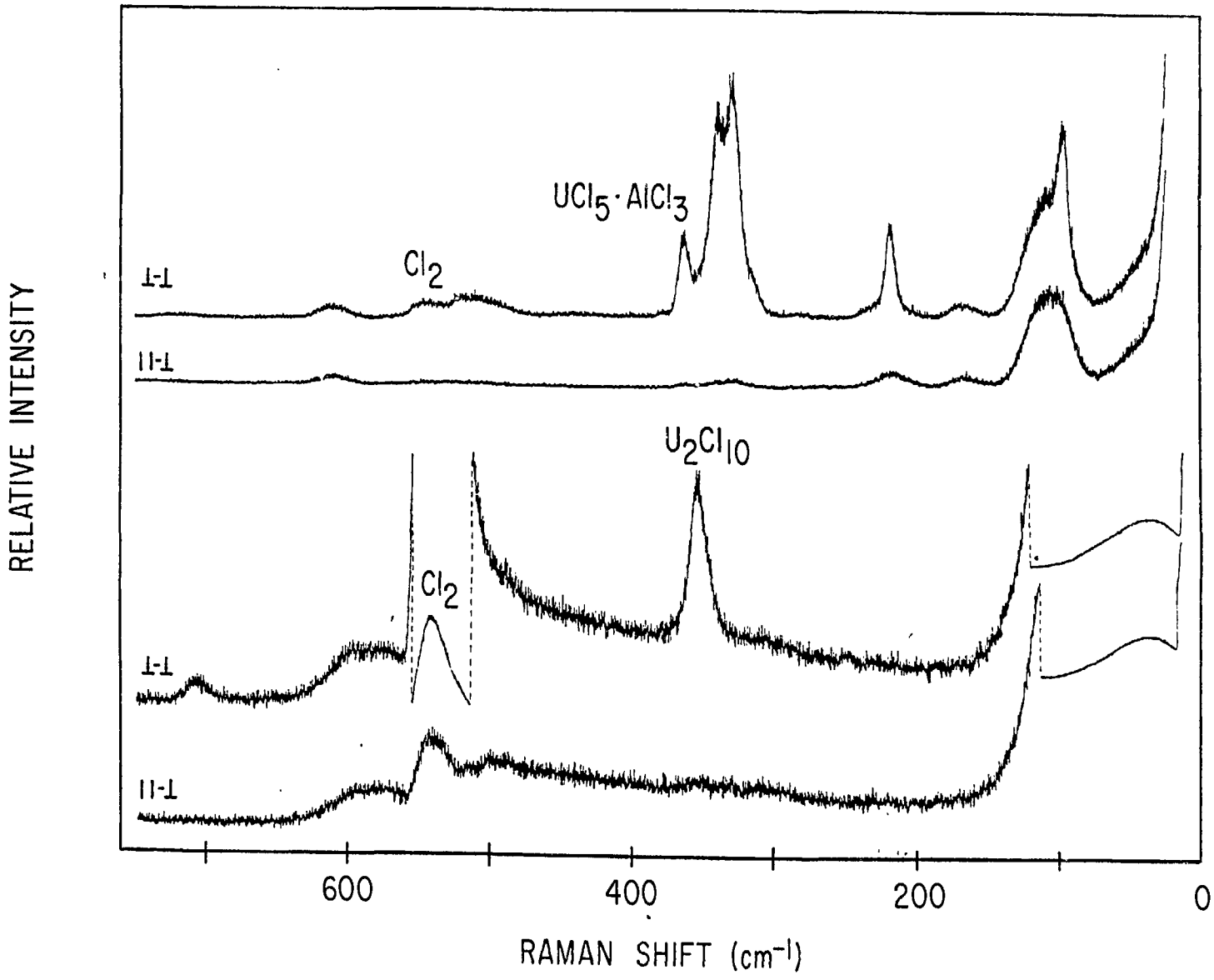
RELATIVE INTENSITY
$UCl_5 \cdot AlCl_3$
Cl_2
U_2Cl_{10}
Cl_2
T-T
II-T
T-T
II-T
600
400
200
0
RAMAN SHIFT (cm^{-1})

Fig. 15

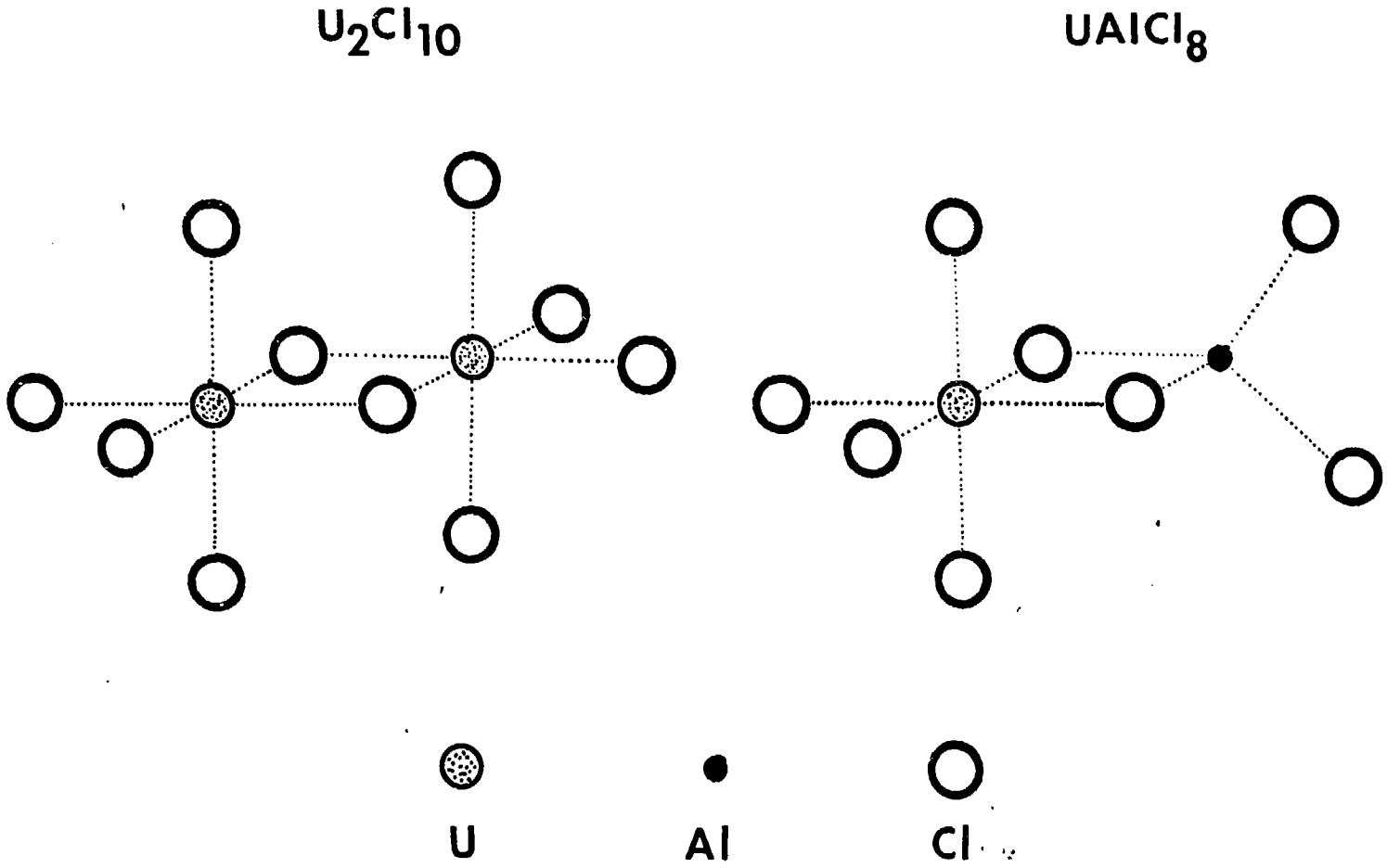

Fig. 16

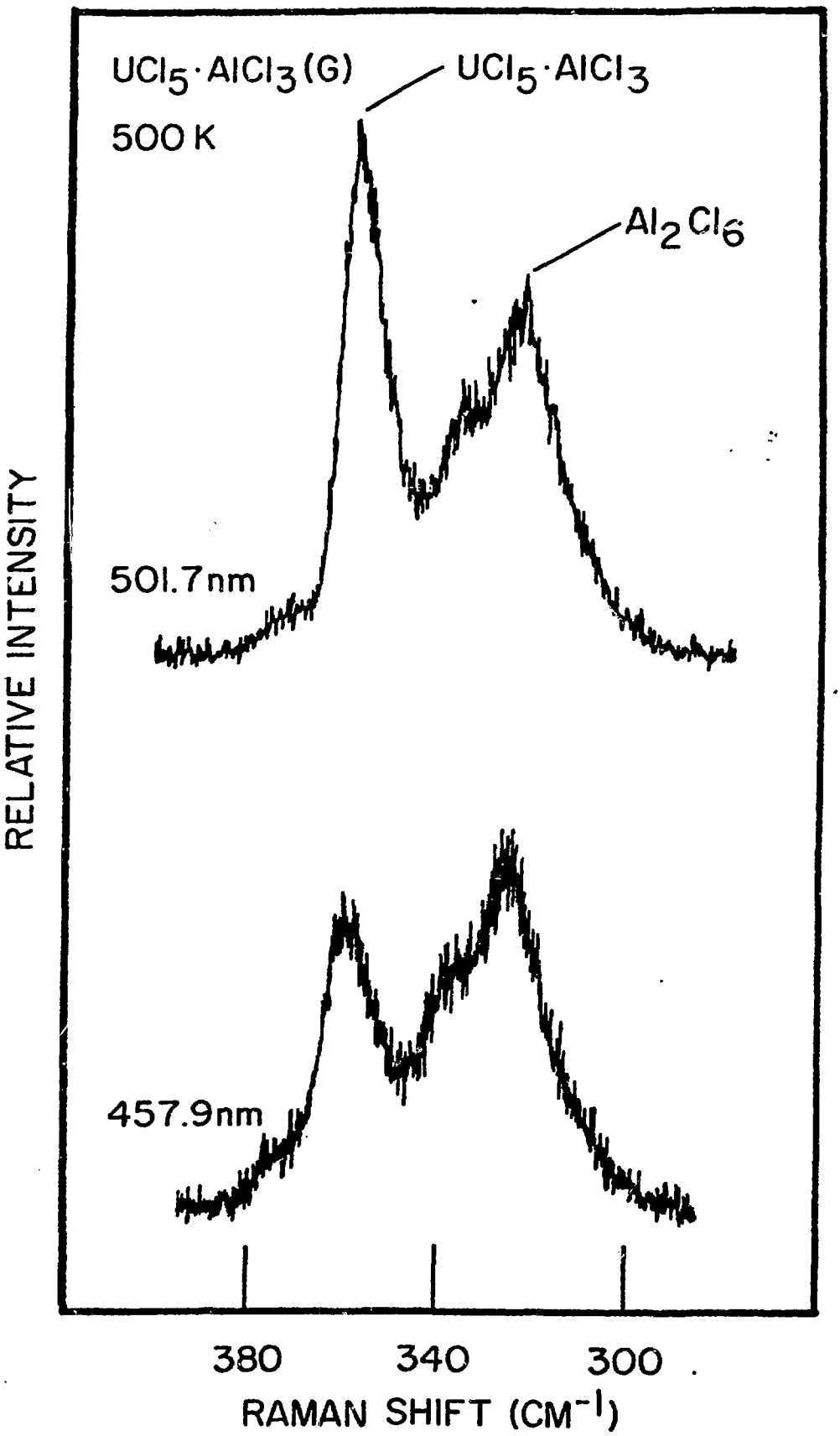
$UCl_5 \cdot AlCl_3$ (G)
500 K
$UCl_5 \cdot AlCl_3$
Al_2Cl_6
501.7nm
457.9nm
RELATIVE INTENSITY
380
340
300
RAMAN SHIFT (CM^{-1})

Fig. 17

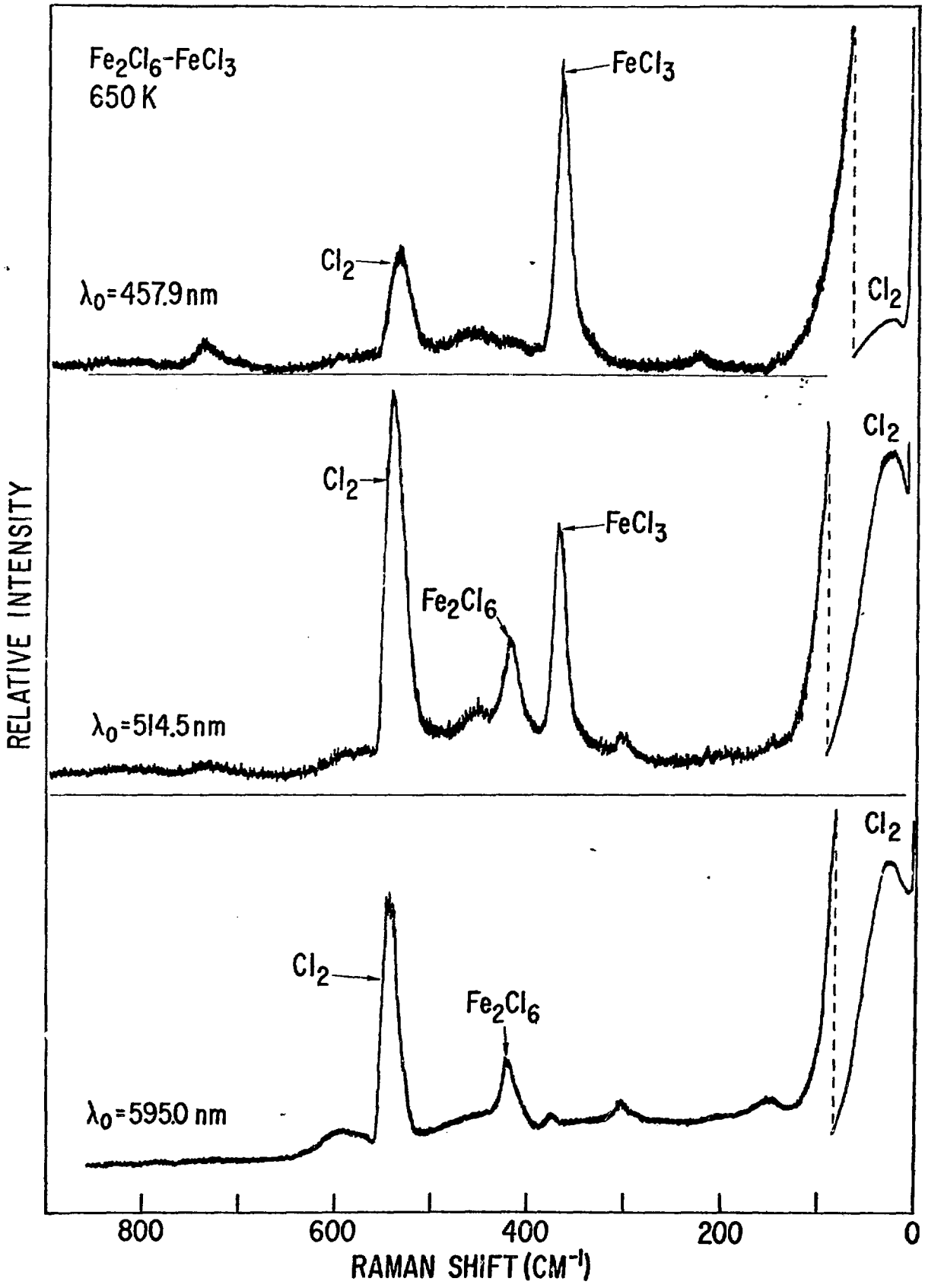
Fe_2Cl_6-$FeCl_3$
650 K
$FeCl_3$
Cl_2
λ_0=457.9nm
Cl_2
Cl_2
Cl_2
$FeCl_3$
Fe_2Cl_6
λ_0=514.5nm
Cl_2
Cl_2
Fe_2Cl_6
λ_0=595.0 nm
RELATIVE INTENSITY
800
600
400
200
0
RAMAN SHIFT (CM^{-1})

Fig. 18

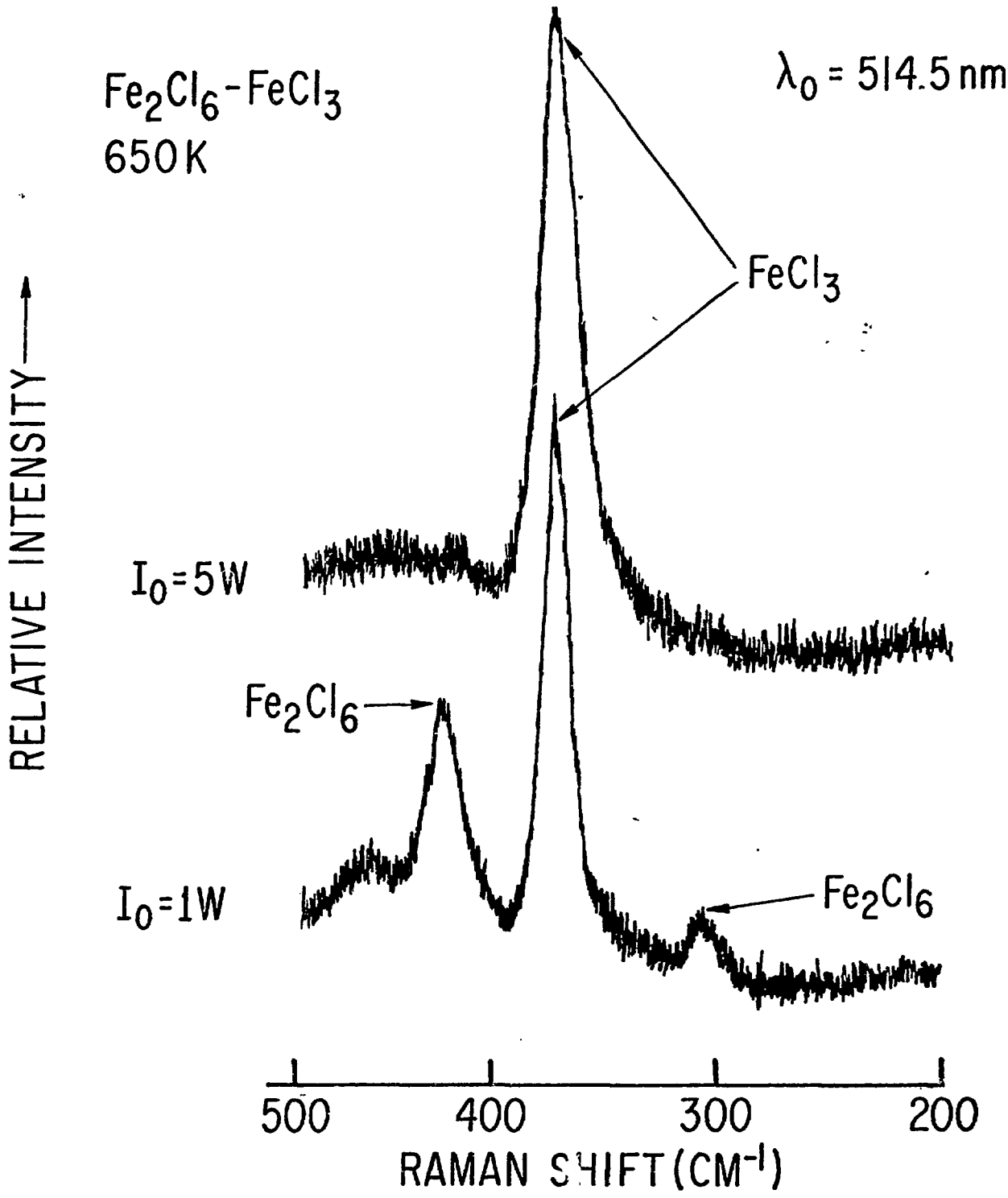
Fe_2Cl_6-$FeCl_3$
650K
λ_0 = 514.5 nm
$FeCl_3$
I_0=5W
Fe_2Cl_6
I_0=1W
Fe_2Cl_6
RELATIVE INTENSITY
500
400
300
200
RAMAN SHIFT (CM^{-1})

Fig. 19

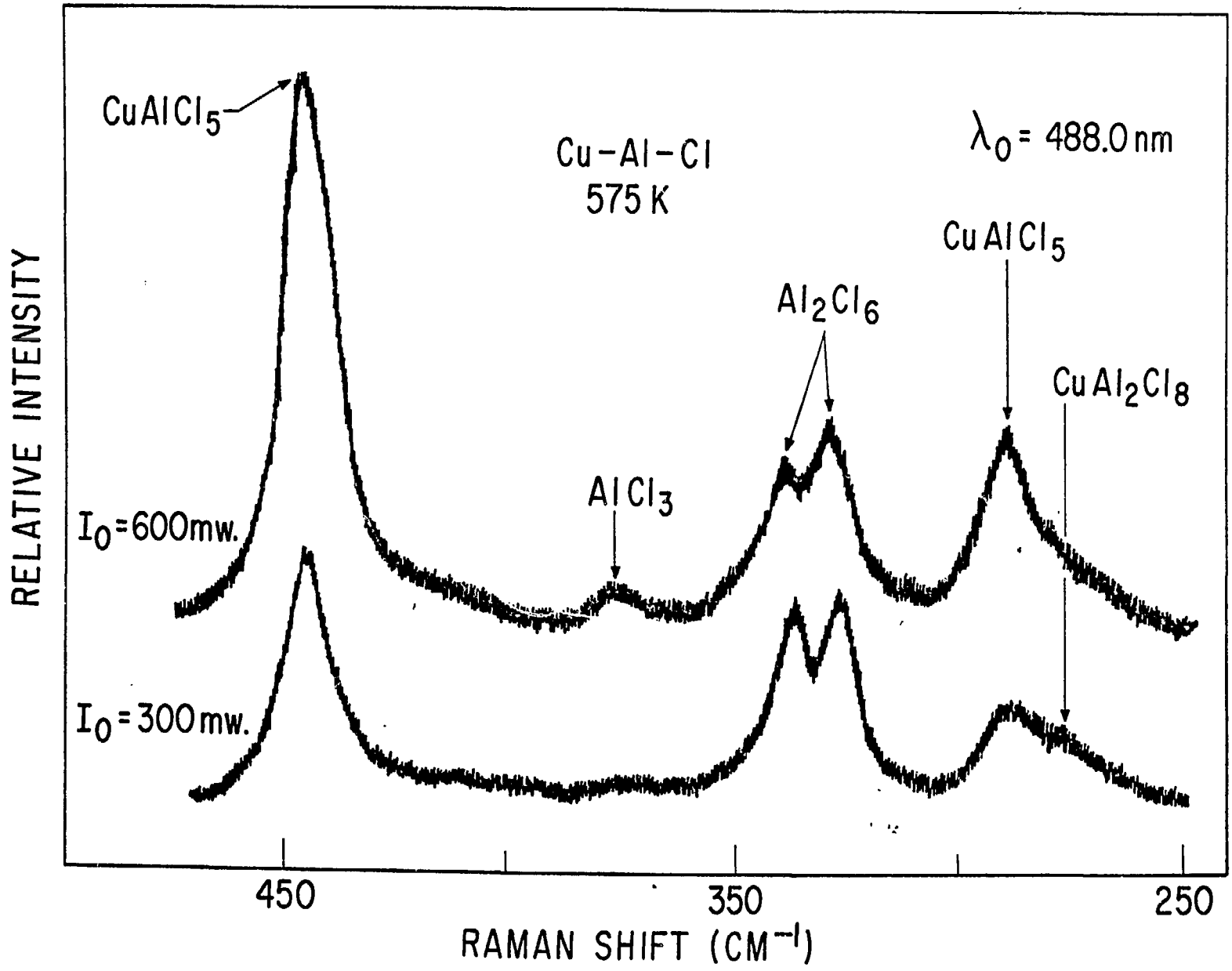
CuAlCl5
Cu-Al-Cl
575 K
λ0 = 488.0 nm
CuAlCl5
Al2Cl6
CuAl2Cl8
AlCl3
I0 = 600 mw.
I0 = 300 mw.
RELATIVE INTENSITY
450
350
250
RAMAN SHIFT (CM-1)

Fig. 20

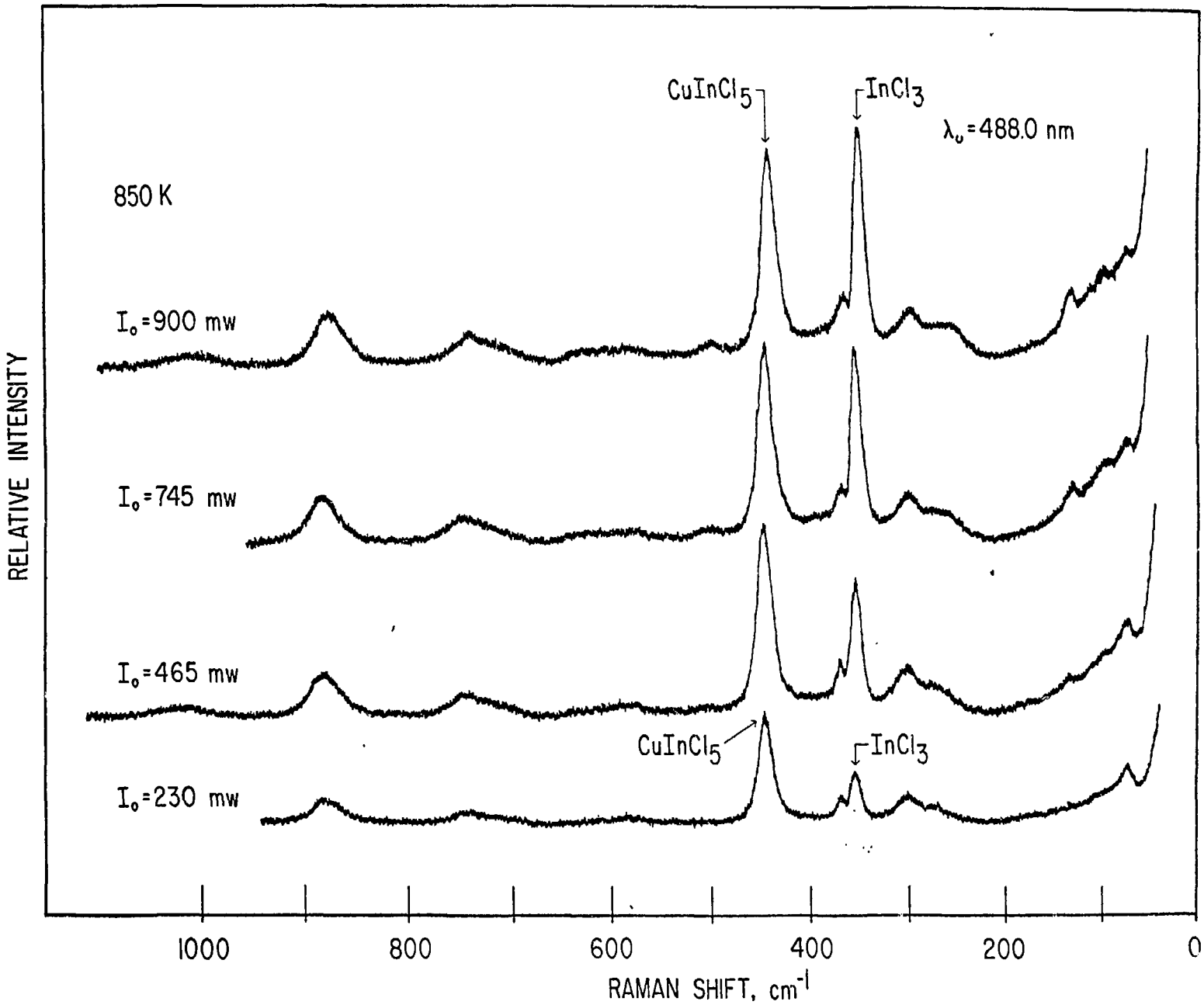
CuInCl5
InCl3
λo=488.0 nm
850 K
Io=900 mw
Io=745 mw
Io=465 mw
Io=230 mw
CuInCl5
InCl3
RELATIVE INTENSITY
1000
800
600
400
200
0
RAMAN SHIFT, cm-1

Fig. 21

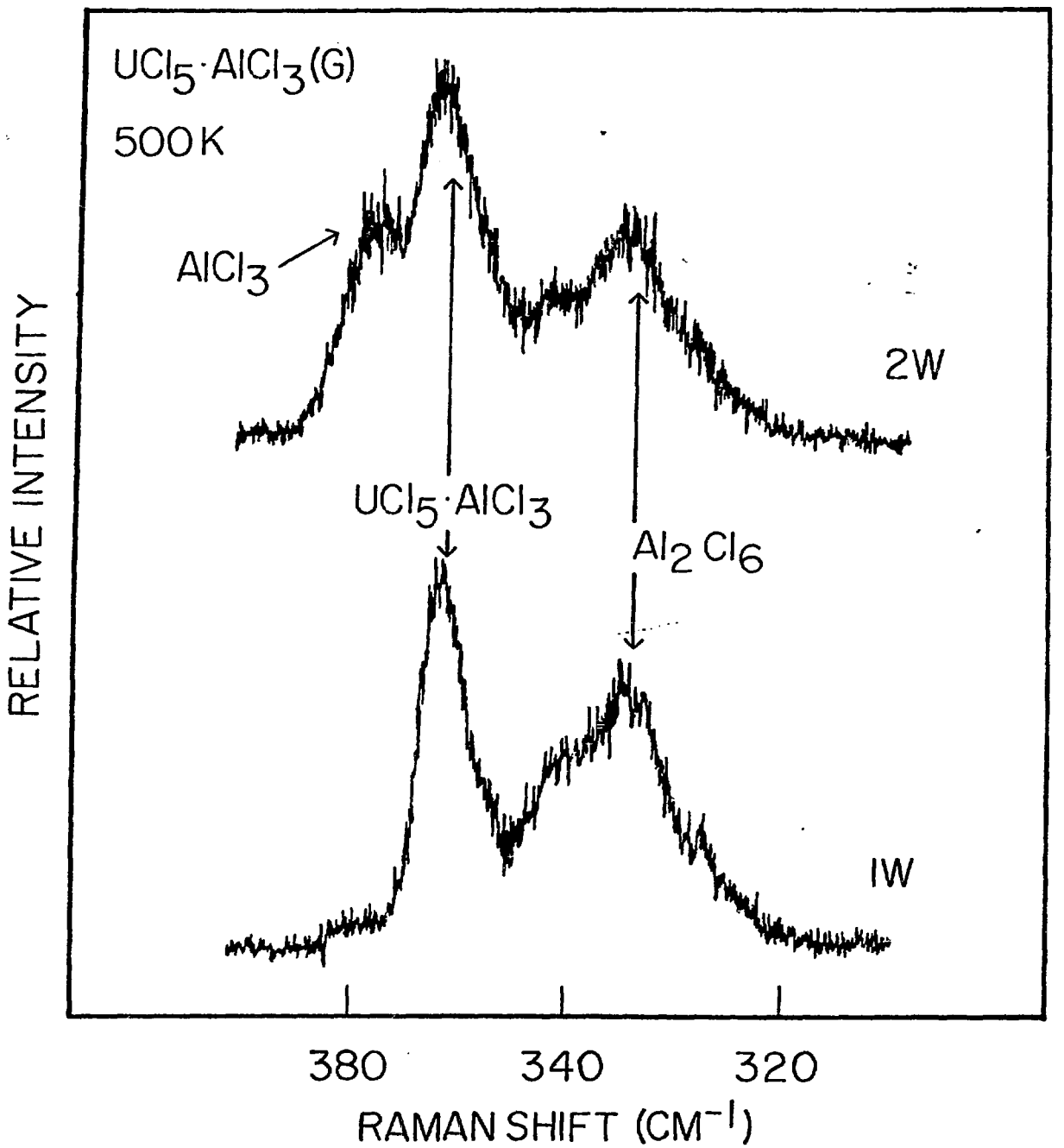
$UCl_5 \cdot AlCl_3$(G)
500K
$AlCl_3$
2W
$UCl_5 \cdot AlCl_3$
Al_2Cl_6
1W
RELATIVE INTENSITY
380
340
320
RAMAN SHIFT (CM^{-1})

Fig. 22